https://doi.org/10.5194/egusphere-2025-2502
Preprint. Discussion started: 21 July 2025

Tracing Water Masses and Particle Dispersion on the Northern South China Sea Shelf Using POM Signatures under Contrasting Wind Conditions: A New Perspective

Jay Lee[1,2], James T. Liu[1*], Yu-Shih Lin[1], Tung-Yuan Ho[3], Chen-Tung Arthur Chen[1], Wenping Gong[4], Chau-Ron Wu[2, 5]

[1]Department of Oceanography, National Sun Yat-sen University, Kaohsiung, Taiwan R.O.C.

[2]Research Center for Critical Issues, Academia Sinica, Taipei, Taiwan R.O.C.

[3]Research Center for Environmental Changes, Academia Sinica, Taipei, Taiwan R.O.C.

[4]School of Marine Sciences, Sun Yat-Sen University, Guangzhou, Guangdong, China

[5]Department of Earth Sciences, National Taiwan Normal University, Taipei, Taiwan R.O.C.

Correspondence to: James T. Liu (james@mail.nsysu.edu.tw)

Tel: +886-7-525-5144, Fax: +886-7-525-5130

https://doi.org/10.5194/egusphere-2025-2502
Preprint. Discussion started: 21 July 2025

Abstract

River-dominated shelf systems are shaped by complex hydrodynamic and biogeochemical interactions, making source-to-sink (S2S) tracking a challenge. To explore the influence of physical processes on particle distribution in the northern South China Sea, two research cruises were conducted along the Guangdong coast in the summers of 2018 and 2020. Hydrographic profiles and particle volume concentrations were measured using a CTD and a laser *in-situ* scattering transmissometer (LISST). Seawater samples from the surface, pycnocline, and bottom layers were analyzed for chlorophyll-a (Chl-a), particulate organic matter (POM, including POC, PN, and $\delta^{13}C_{POC}$), and nutrients. Empirical orthogonal function (EOF) analysis revealed distinct patterns of hydrodynamic control in both years. In 2018, stratification was intensified by local rainfall from a cyclonic system and the subsurface seawater, leading to the accumulation of larger particles at the pycnocline. In 2020, however, the Zhujiang River plume (ZRP) played a dominant role in stabilizing the water column under the southwesterly monsoon, entraining bio-particles enriched in $\delta^{13}C_{POC}$. This process facilitated the northeastward transport of biogenic material into the Taiwan Strait, possibly influencing sediment composition along the plume pathway. Although the ZRP and subsurface chlorophyll maximum shared similar biogeochemical signatures, the ZRP exhibited higher POC-to-Chl-a ratios and greater particle bulk densities, indicating more advanced POM degradation. Notably, the significantly negative correlation between $\delta^{13}C_{POC}$ and salinity along the ZRP highlights $\delta^{13}C_{POC}$ serves as a robust tracer of riverine water, more effective than the traditional N/P ratio in this river-dominated shelf system.

Keywords: River-dominated shelf regions, Zhujiang River plume, subsurface chlorophyll maximum, water stratification, particle bulk density, POC-to-Chl-a ratio, $\delta^{13}C_{POC}$.

https://doi.org/10.5194/egusphere-2025-2502
Preprint. Discussion started: 21 July 2025

1. Introduction

As one of the world's largest river-dominated ocean margins (RiOMar; Xie et al., 2020), the northern South China Sea (NSCS) receives substantial inputs of particulate matter and terrestrial nutrients from major rivers, most notably the Zhujiang (Pearl) River (Cai et al., 2004; Lee et al., 2006; Liu et al., 2012; Ou et al., 2019; Xu et al., 2008). These riverine effluents contribute to the diversity of water masses and suspended particle assemblages, resulting in complex hydrographic structures in nearshore regions (Lan et al., 2009; Yin et al., 2004; Zhou et al., 2012). The hydrodynamics and biogeochemical processes governing the dispersal of these effluents play a critical role in shaping coastal ecosystems, contributing to phenomena such as benthic hypoxia along the river plume pathway (Luo et al., 2023; Qian et al., 2018).

The distribution of the Zhujiang River plume (ZRP) on the continental shelf is highly dynamic, shaped by factors such as river discharge, wind patterns, upwelling, and coastal flow fields (Chen et al., 2016; Dong et al., 2004; Lee et al., 2021; Ou et al., 2009; Xu et al., 2019; Zu et al., 2014; Zu et al., 2015). Satellite-based turbidity imagery has identified eight distinct spreading patterns of the ZRP (Chen et al., 2017a). During the summer monsoon, southwesterly winds drive a northeastward surface flow, facilitating the propagation of the ZRP along the Guangdong coast (Chen et al., 2017a, b; Lee et al., 2021; Pan et al., 2014; Zu et al., 2014). Monsoon-driven coastal upwelling further enhances this transport by generating baroclinic jet currents at the interface between the freshwater plume and the underlying saltwater (Chen et al., 2017b; Zu et al., 2015).

The ZRP is critical in regulating nutrient availability and supporting primary production in the NSCS. (Liu et al., 2019; Tong et al., 2024; Yang et al., 2021; Yin et al., 2001, 2004). Strong water stratification inhibits vertical mixing along the plume pathway, allowing the riverine substances to be transported over long distances (Chen et al., 2017b; Harrison et al., 2008; Horner-Devine et al., 2015; Lee et al., 2021; Shu et al., 2014). Underway salinity observations and satellite imagery confirm the broad extent of the ZRP into the southern Taiwan Strait (Bai

https://doi.org/10.5194/egusphere-2025-2502
Preprint. Discussion started: 21 July 2025

et al., 2015). Various methods have been used to investigate hydrographic, hydrodynamic, and biogeochemical responses associated with the ZRP (Gu et al., 2017; Harrison et al., 2008; Lan et al., 2009; Yin et al., 2004; Zu et al., 2015). A distinctive biogeochemical characteristic of the Zhujiang River is its high nitrogen-to-phosphorus (N/P) ratio, which contrasts with that of the surrounding seawater in the NSCS (Lee et al., 2023; Xu et al., 2008; Yin et al., 2001). The influx of nitrogen-rich riverine water into the nitrogen-limited NSCS significantly enhances coastal biomass, as observed by ocean color satellite sensors (Chen et al., 2004; Xu et al., 2008).

This phytoplankton bloom not only modifies planktonic communities but also alters the physicochemical properties of suspended particles in shallow waters (Jiang et al., 2015; Li et al., 2018; Zhong et al., 2021). The signatures of particulate organic matter (POM) serve as valuable proxies for understanding biogeochemical cycles in the global ocean system (SCOR Working Group, 2007; Weaver, 1991) and the source-to-sink (S2S) transport mechanisms of riverine materials (Fischer, 1991; Gu, 2009; Meyers et al., 1993; Sun et al., 2021). While particulate matters are generally expected to retain its original characteristics during transport (Allen, 2017), it can undergo significant transformations along the way (Allen, 2017; Lee et al., 2023; Turner et al., 2002). Flocculation promotes particle aggregation, altering size distribution and bulk density, which subsequently impacts the removal of substances from the water column (Hill et al., 2000). Riverine nutrient inputs stimulate phytoplankton growth, reshaping biological community composition (Jiang et al., 2015; Lu et al., 2009; Tong et al., 2024; Zhong et al., 2021) and influencing POM characteristics, such as stable isotope compositions and C/N ratios, which are commonly used as indicators for tracing particle sources in routing systems. (Miller et al., 2008; Yin et al., 2001). For instance, phytoplankton blooms often lead to $\delta^{13}C$ enrichment in POM due to the progressive depletion of ^{12}C in the dissolved inorganic carbon pool of the surrounding seawater (Deuser, 1970; Nakatsuka et al., 1992). Microbial degradation further alters POM composition, resulting in residual POM with a relatively $\delta^{13}C$-depleted signature (Close et al., 2020; Huang et al., 2021). Additionally,

https://doi.org/10.5194/egusphere-2025-2502
Preprint. Discussion started: 21 July 2025

coastal hydrodynamics add further complexity to the physicochemical properties of suspended particles (Eisma, 1986; Manning et al., 2010). Turbulence from waves and currents enhances mixing, incorporating materials from surrounding waters along dispersal pathways (Cross et al., 2014; Jago et al., 2006; Petersen et al., 1998). As a result, the original characteristics of riverine materials might not persist throughout the S2S system.

Our previous study near the Zhujiang River estuary (Lee et al., 2023) revealed distinct differences in the particle characteristics between the proximal ZRP and surrounding marine waters. However, the NSCS is influenced by strong physical processes, including basin-wide circulation, upwelling, and nonlinear internal waves (Alford et al., 2015; Feng et al., 2021; Gan et al., 2022; Guo et al., 2014; Jing et al., 2009; Lee et al., 2021; Su, 2004). It remains unclear whether the biogeochemical distinctions associated with the ZRP are preserved as it spreads across the broader NSCS shelf. To enhance our understanding of particulate matter transport on the NSCS shelf, this study addresses three key questions:

1. How do hydrodynamic processes influence the distribution of particulate matter in a river-dominated shelf system?
2. What biogeochemical signatures of the suspended particles are carried by the ZRP along its dispersal pathway, and which ones are transported to the downstream regions, such as the Taiwan Strait?
3. Given that dissolved tracers (e.g., salinity, dissolved inorganic carbon) have been widely used to identify ZRP waters (Bai et al., 2015; Cao et al., 2011; Guo et al., 2008; Huang et al., 2020), can particulate matter, despite its non-conservative nature, also serve as a meaningful indicator of water mass influence and associated biogeochemical processes (Bouillon et al., 2007, 2011; Cathalot et al., 2013)?

2. Materials and methods

2.1 Hydrographic measurements and water sampling

https://doi.org/10.5194/egusphere-2025-2502
Preprint. Discussion started: 21 July 2025

Two research cruises were conducted in the summers of 2018 (August 19-22, aboard R/V Ocean Researcher III; ORIII) and 2020 (July 22–28, aboard R/V Legend) along the Guangdong coast under varying river discharge conditions (Fig. 1a, d). Seven hydrographic stations (ZHJ3-L1) were established to assess the spatial variability in hydrodynamics and the physicochemical properties of suspended particles along the river plume dispersal pathway (Fig. 1b, e). To capture temporal variability induced by internal waves and tidal flows (Lee et al., 2021, 2023), 24-hour time-series measurements with hourly sampling were conducted at Station K1 in 2018 and Station L1 in 2020 (Fig. 1b, e). However, due to technical issues, no data were collected at the two southwest-most stations (ZHJ3 and ZHJ4) in 2018.

At each station, a Seabird SBE 19 plus CTD rosette was deployed to measure salinity, temperature, water density, and fluorescence. The CTD was operated with a sampling rate of 0.04 seconds with a lowering rate of 0.5 m s^{-1}. To reduce high-frequency noise in the hydrographic profiles, data points collected within 0.2 meters were averaged into a single measurement. Additionally, a laser *in-situ* scattering transmissometer (LISST-200X, Sequoia Scientific, Inc., Bellevue, USA) was mounted on the rosette to measure the volume concentration (VC) of suspended particles across 32 grain-size classes, ranging from 2.5 to 500 µm.

Seawater samples were collected from three depths: 3 m below the surface, at the pycnocline, and 3 m above the seabed, using 10 L water samplers on the CTD rosette (Niskin bottles in 2018 and Go-Flo bottles in 2020). After collection, 150 mL of seawater was filtered through a 0.45 µm Millex®-LCR syringe filter to analyze dissolved nutrients and was immediately frozen in liquid nitrogen. Additionally, two 500 mL seawater samples were collected and stored in HDPE opaque amber bottles. onboard water samples were filtered using pre-combusted glass fiber filters (GF/F, Whatman; diameter: 25 mm; pore size: 0.7 µm; pre-combusted at 500°C for 6 hours) for subsequent analyses of suspended sediment concentration (SSC), chlorophyll-a (Chl-a), and POM. Chl-a samples were wrapped in aluminum foil to prevent light exposure,

https://doi.org/10.5194/egusphere-2025-2502
Preprint. Discussion started: 21 July 2025

and the results were used to validate fluorescence measurements from the CTD profile (Appendix Fig. A1). All filtered samples were stored at temperatures below -4 °C during the cruise before being processed in the laboratory.

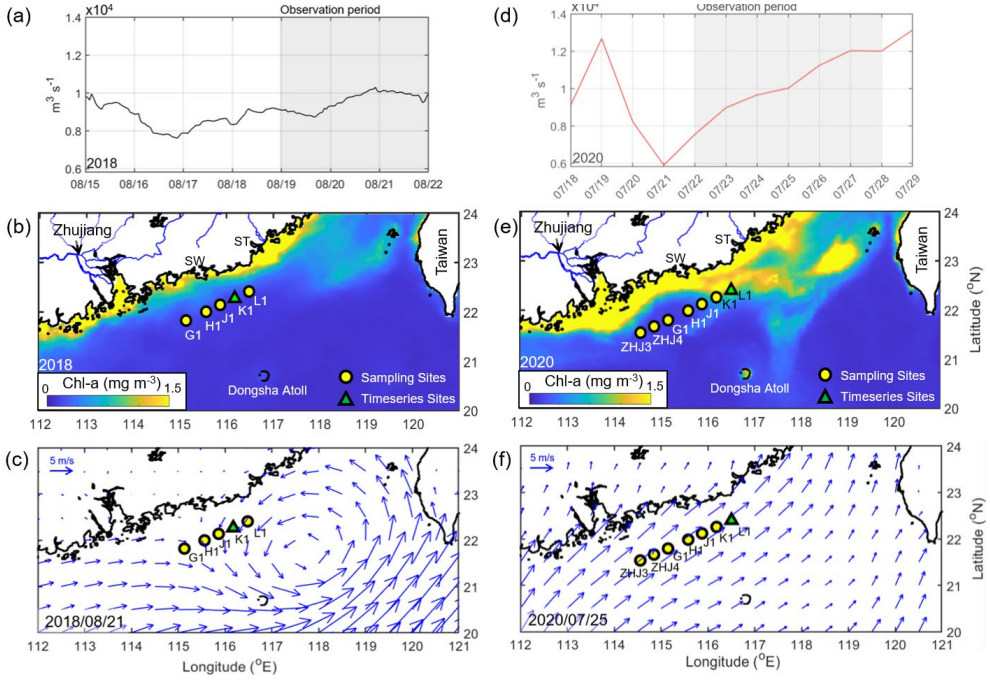

Figure 1: Environmental conditions during the observation period. Panels from top to bottom display Zhujiang River discharge (a, d), ocean color images from MODIS (b, e), and 10-meter wind fields (c, f). Data from 2018 are shown on the left, and 2020 data are on the right. The gray shading in the river discharge panel indicates the observation period during the cruise. The color scale in the MODIS satellite image represents Chl-a concentration. To represent the average Chl-a distribution in the NSCS during the cruise periods, satellite data collected over the corresponding observations were averaged. The "SW" and "ST" shown in the image represent Shanwei and Shantou. Arrows in the wind field panels indicate wind strength and direction. Yellow circles and green triangles denote hydrographic stations, with green triangles representing time-series stations. River discharge data were sourced from the Pearl River Water Resources Commission, satellite data from NASA Worldview (https://worldview.earthdata.nasa.gov/), and wind field data from ECMWF Reanalysis v5 (https://www.ecmwf.int/en/forecasts/dataset/ecmwf-reanalysis-v5).

https://doi.org/10.5194/egusphere-2025-2502
Preprint. Discussion started: 21 July 2025

2.2 Water stratification

Water column stability was quantified using a static stability index, E, a widely used metric for assessing stratification influenced by freshwater input in nearshore environments (Boyer et al., 2005; Du and Liu, 2017; Lee et al., 2016, 2023; Liu et al., 2018b; Lynn and Reid, 1968; Neumann, 1966). The index is defined as:

$$E = (-1/\rho_0) \times (\partial\rho/\partial z) \quad (1)$$

where ρ_0 is the average water density during the observation; ρ is the measured water density at the specific water depth, z. Higher values indicate stronger water stratification, while lower values suggest weaker or well-mixed conditions.

2.3 Nutrient analyses

Nutrient samples collected in 2018 were analyzed at National Sun Yat-sen University, Kaohsiung, while those from 2020 were analyzed at Academia Sinica, Taipei. Nutrient concentrations were calculated using colorimetric methods: phosphate (PO_4^{3-}) and silicate (SiO_4^-) by the molybdenum blue and silicomolybdic acid blue methods, respectively (Fanning et al., 1973; Mullin et al., 1955; Murphy et al., 1962; Pai et al., 1990a; Rimmelin et al., 2005); nitrite (NO_2^-) by the pink azo dye method (Pai et al. 1990b, 2021; Schnetger et al., 2014; Strickland 1972); and nitrate (NO_3^-) by the cadmium-copper reduction method in 2018 and the VCl_3 reduction method in 2020, (Pai et al., 2021; Schnetger et al. 2014). Calibration in 2018 used CSK standards (Wako Pure Chemicals Ltd., Japan) and certified reference materials (KANSO Technos Co., Ltd., Japan), achieving precisions of ±0.05 µmol L^{-1} for phosphate, ±0.1 µmol L^{-1} for silicate, ±0.02 µmol L^{-1} for nitrite, and ±0.08 µmol L^{-1} for nitrate, respectively. In 2020, Merck-certified standard solutions (Merck KGaA, Darmstadt, Germany) were used for nutrient calibration: nitrite (catalog number 1.19899.0500), nitrate (catalog number 1.19811.0500), phosphate (catalog number 1.19898.0500), and silicate (catalog number 1.70236.0500). All calibration standards were prepared using Milli-Q water® to minimize

https://doi.org/10.5194/egusphere-2025-2502
Preprint. Discussion started: 21 July 2025

potential matrix effects. Analytical accuracy and consistency were validated by analyzing an inserted CSK (Certified Standard for Nutrients in Seawater) reference standard during sample runs. Calibration linearity ($R^2 > 0.997$) was confirmed prior to sample analysis. The analytical precisions were ±0.001 μmol L^{-1} for nitrite, ±0.016 μmol L^{-1} for nitrate, ±0.01 μmol L^{-1} for phosphate, and ±0.1 μmol L^{-1} for silicate.

2.4 Identification of suspended particle characteristics

2.4.1 Physical properties of suspended particles

LISST measured the VC of 32 size classes with non-uniform bin size increments (larger increments in the coarser size classes). Therefore, VC records were normalized (VC_{nor}; Jouon et al. 2008) using the following equation to represent the particle size composition:

$$VC_{nor,i} = VC_{mea,i}/\mathrm{diff}(BS_i) \quad (2)$$

where i indicates each size class; VC_{mea} is the measured VC; BS is the corresponding bin size.

The SSC was determined by weighing the filter after freeze-drying for over 24 hours. The SSC and VCs were then used to calculate the particle bulk density (ρ_{bk}) applying the following equation (Hsu et al., 2010):

$$\rho_{bk} = \rho_{IW} + (1 - \rho_{IW}/\rho_p) \times (SSC/VC) \quad (3)$$

where the ρ_{IW} is the average seawater density measured along the transect in two cruises (1,023 kg m^{-3} in this study); ρ_p is the assumed density of the solid part of the particle (2,650 kg m^{-3}).

2.4.2 Biogeochemical properties of suspended particles (POM and Chl-a)

In the pre-processing of POM analysis, the weighed filter was treated with 2N HCl to remove inorganic carbon, followed by rinsing with Milli-Q water® to eliminate residual acid. POM analysis was conducted using an elemental analyzer coupled with an isotope ratio mass spectrometer (Flash 2000 and Delta V Plus; both from Thermo Fisher Scientific). Calibration of isotopic ratios and precision assessments were performed using internationally certified standards (USGS40, USGS43, USGS64, USGS73, and NIST8542) and soil standards

https://doi.org/10.5194/egusphere-2025-2502
Preprint. Discussion started: 21 July 2025

(certificate number 341506; Thermo Fisher Scientific). The relative precision was maintained at ±5% for particulate organic carbon (POC; 1σ) and particulate organic nitrogen (PN; 1σ). The absolute precision was within ±0.3‰ for $\delta^{13}C_{POC}$.

Chl-a was extracted from the retained particles on the filter by immersing the filter in 90% acetone within a 15 mL centrifuge tube at 4°C for 24 hours. The Chl-a concentration was then quantified using a 10-AU Field Fluorometer (Turner Designs). To prevent photodecomposition of Chl-a, the procedure was conducted in a subdued light environment. The measured Chl-a concentration was used to calculate the PC ratio (particulate organic carbon to Chl-a concentration), which serves as an indicator of POM degradation (Guo et al., 2015; Jakobsen et al., 2016; Taylor et al., 1997). Guo et al. (2015) identified a PC ratio of 200 as the threshold between degraded and fresh POM. A lower PC ratio indicates fresh or newly produced POM, whereas a higher ratio suggests more degraded POM.

$$\text{PC ratio} = \text{POC/Chl-a} \quad (4)$$

2.5 River discharge and open-source data

River discharge from the Zhujiang River was measured at gauging stations on its three major tributaries: Samsui on the North River, Makou on the West River, and Bolou on the East River. Since data for Bolou was unavailable in 2018 and the East River's minimal contribution to total flow (Zhang et al., 2012), Bolou's measurements were excluded to ensure consistency between the 2018 and 2020 datasets. Daily average discharge values were used to filter out high-frequency variability. All data were obtained from the Zhujiang River Water Resources Commission (https://www.pearlwater.gov.cn/).

Ocean-color satellite imagery was obtained from NASA's Worldview application (https://worldview.earthdata.nasa.gov), providing daily Chl-a data at a horizontal resolution of 1/24° × 1/24°. To represent the overall Chl-a distribution in the NSCS, satellite data collected during each cruise were averaged. Surface water samples provided ground truth data to validate

https://doi.org/10.5194/egusphere-2025-2502
Preprint. Discussion started: 21 July 2025

the accuracy of satellite-derived Chl-a measurements.

Precipitation data were obtained from the Integrated Multi-satellite Retrievals for Global Precipitation Measurement (NASA), with a horizontal resolution of 1/10° × 1/10° and daily observation intervals (https://disc.gsfc.nasa.gov/; Huffman et al., 2023). Wind field data at 10 meters above the surface were sourced from the ECMWF Reanalysis v5 dataset (https://www.ecmwf.int/en/forecasts/dataset/ecmwf-reanalysis-v5).

3. Results

3.1 River runoff and hydrographic changes on the NSCS shelf

Our gauging station data are consistent with historical records showing that the average river runoff during the wet season typically ranges between 1 and 2 × 10^4 m^3 s^{-1} (Hong et al., 2020; Zhang et al., 2012; Fig. 1a, d). During the sampling periods, river discharge conditions were generally comparable between 2018 and 2020, with average values of 0.96 × 10^4 m^3 s^{-1} and 1.02 × 10^4 m^3 s^{-1}, respectively. Although differences were observed, they are unlikely to fully account for the greater offshore extent of the ZRP in 2020 (Fig. 1b, e). Instead, contrasting wind forcing played a dominant role in shaping the plume dispersal patterns. Enhanced southwesterly winds during the 2020 summer monsoon (Fig. 1c, f) promoted stronger northeastward propagation of the ZRP, facilitating its spread toward the southern Taiwan Strait, as evidenced by satellite imagery (Fig. 1e). Additional mechanisms, such as variability in river discharge influenced by dam operations and climatic oscillations (ENSO and PDO; Gu et al., 2017; Liu et al., 2018a; Ouyang et al., 2014; Zhou et al., 2021), may have also contributed to long-term variability but were likely secondary factors during our observation periods.

The dispersal of the ZRP created distinct hydrographic structures in the shallow water environment in 2018 and 2020 (Fig. 2). Salinity profiles in 2018 indicated the presence of fresh water (salinity 33–34) in the upper water column, primarily due to heavy precipitation induced by a tropical depression (Fig. 1c, Fig. 2a, and Appendix Fig. A2). Despite lower offshore rainfall in 2020, a water mass with salinity below 33 was observed at depths shallower than 7

https://doi.org/10.5194/egusphere-2025-2502
Preprint. Discussion started: 21 July 2025

m from Stations K1 to L1 (Fig. 2e). Temperature profiles in both years exhibited a typical two-layer structure with warm water (>25°C) restricted to depths shallower than 50 m (Fig. 2b, f), consistent with previous observations in the NSCS (Lee et al., 2021; Wong et al., 2015; Zeng et al., 2016). Vertical water stability revealed a continuous stratified layer around 25 m on the shelf in 2018 (E > 0.005; Fig. 2c), attributed to low-salinity, warm surface water. In contrast, the stratification structure in 2020 was discontinuous along the transect, despite the presence of a warm surface layer. With the ZRP input, strong stratification was observed on the eastern side of the transect (Fig. 2g).

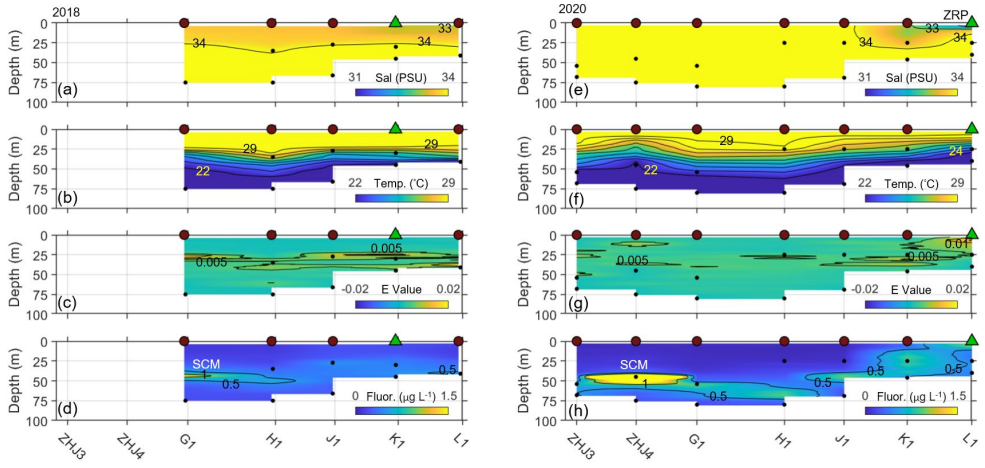

Figure 2: Hydrographic profiles along the transect in 2018 (left) and 2020 (right). Panels from top to bottom show salinity, temperature, E values, and fluorescence. Brown circles and green triangles mark hydrographic stations (as in Fig. 1), while black dots indicate sampling depths. "SCM" represents the subsurface chlorophyll maximum, and "ZRP" denotes the Zhujiang River plume.

Dissolved nutrient distributions also showed distinct patterns in both years, with concentrations generally increased with depth, displaying lower values near the surface (Fig. 3). In 2018 (2020), silicate concentrations ranged from 1.8 (0.6) to 16.1 (9.2) μM, nitrate + nitrite (N) from 0.03 (0.13) to 9.18 (6.65) μM, and phosphate from 0.01 (<0.01) to 0.75 (0.48) μM. Bottom concentrations in 2018 were nearly double those measured in 2020. However,

https://doi.org/10.5194/egusphere-2025-2502
Preprint. Discussion started: 21 July 2025

surface nutrient concentrations at Station L1 significantly increased in 2020, reaching 7.32 µM for silicate, 5.11 µM for nitrate + nitrite, and 0.37 µM for phosphate, indicating shifts in water-mass composition. The N/P ratio, a conventional indicator of the water mass, generally remained below 15 along the transect for both years (Table 1). Exceptionally high N/P values were observed in 2020 (e.g., 88.43 at Station ZHJ4 and 89.47 at Station J1). Conversely, the surface water at Station L1 exhibited relatively lower N/P values (14.01 in 2020), despite the ZRP being characterized by significantly high N/P ratios due to low phosphate concentrations in river runoff (Yin et al., 2001).

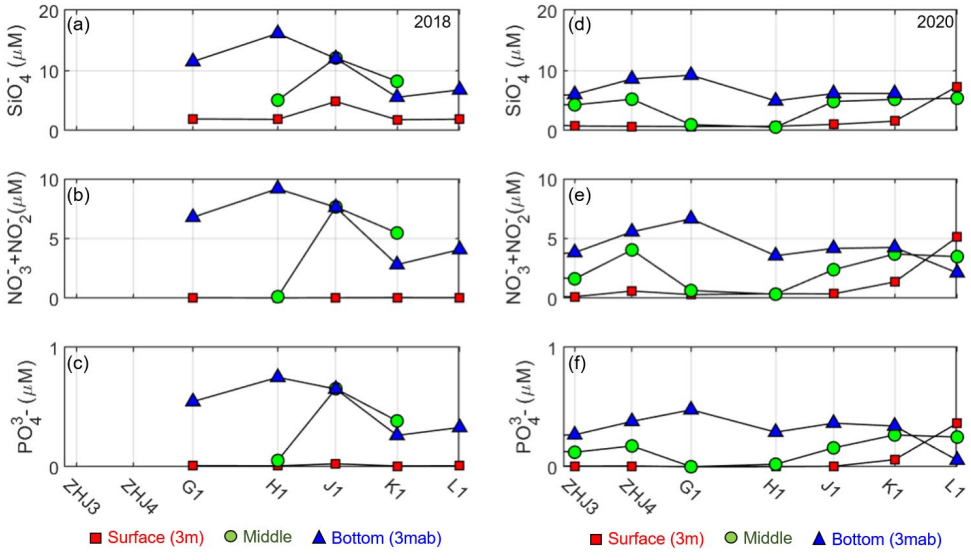

Figure 3: Nutrient concentrations along the transect in 2018 (left) and 2020 (right). Panels show (a, d) silicate, (b, e) nitrate + nitrite, and (c, f) phosphate. Colored points represent samples collected at different depths (red square: surface; greed circle: middle; blue triangle: 3 meter above bottom).

https://doi.org/10.5194/egusphere-2025-2502
Preprint. Discussion started: 21 July 2025

Table 1: Calculated N/P ratios for 2018 (top table) and 2020 (bottom table) at each hydrographic site.

2018

N/P Ratio	ZHJ3	ZHJ4	G1	H1	J1	K1	L1
Surface	-	-	4.20	3.75	1.72	8.14	4.89
Middle	-	-	12.26	2.42	11.70	14.23	12.19
Bottom	-	-	12.40	12.25	11.69	10.70	12.39

* "-" symbol indicates missing or error data.

* Gray value indicates the N or P under the detection limit.

2020

N/P Ratio	ZHJ3	ZHJ4	G1	H1	J1	K1	L1(ZRP)
Surface	22.18	88.43	-	368.31	89.47	22.69	14.01
Middle	13.29	23.18	626.08	15.59	15.10	13.87	13.99
Bottom	14.28	14.64	13.93	12.26	11.43	12.44	38.02

* "-" symbol indicates missing or error data.

* Gray value indicates the N or P under the detection limit.

https://doi.org/10.5194/egusphere-2025-2502
Preprint. Discussion started: 21 July 2025

3.2 Contrasting POM Features in the Shelf System

The subsurface chlorophyll maximum (SCM) was observed at depths of 40–75 m from Stations ZHJ3 to H1 in both years (Fig. 2d, h). Peak fluorescence reached 1.26 μg L^{-1} in 2018 and 5.43 μg L^{-1} in 2020. Chl-a measurements followed a similar trend (Fig. 4), with a maximum concentration of 2.79 μg L^{-1} recorded at Station ZHJ4 in 2020. These findings suggest a significant presence of phytoplanktonic biomass within the SCM, further supported by elevated POC concentrations (Appendix Fig. A3). POM analysis revealed significantly lighter $\delta^{13}C_{POC}$ values (below -30‰; Fig. 5c) in the SCM water relative to ambient seawater, indicating distinct isotopic fractionation during phytoplankton uptake and biodegradation (Close et al., 2020; Tuerena et al., 2019; Zhang et al., 1999). Similar $\delta^{13}C_{POC}$ depletion has been reported on the East China Sea shelf, attributed to phytoplankton size composition and the intrusion of the offshore water having a low $\delta^{13}C_{POC}$ value (Liu et al., 2018c).

A significant increase in fluorescence was also observed in the upper water at Station L1 in 2020, which was absent in 2018 (Fig. 2d, h). This difference was attributed to the input of nutrient-rich ZRP water, which stimulated phytoplankton growth (Fig. 1a, e and Fig. 3; Yin et al., 2001, 2004; Yu et al., 2020). Consequently, surface waters in 2020 exhibited Chl-a concentrations exceeding 1 μg L^{-1} (Fig. 4c), which led to altered POM properties, including relatively enriched $\delta^{13}C_{POC}$ values (> -24.5‰; Fig. 5c). To rule out potential temporal aliasing from hydrodynamic forcing (e.g., nonlinear internal waves or tidal flows; Alford et al., 2015; Guo et al., 2014; Lee et al., 2021; Zu et al., 2015), a 24-hour continuous observation of Chl-a and $\delta^{13}C_{POC}$ was compared with surface salinity (averaged within the top 5 m; Fig. 4b, d and 5b, d). In 2018, Chl-a and $\delta^{13}C_{POC}$ concentrations remained stable at approximately 0.5 μg L^{-1} and -25.4‰, respectively, with an average salinity of 33.3. In contrast, surface Chl-a concentrations in 2020 were more than twice those at the bottom, showing an inverse correlation with salinity. Meanwhile, bottom Chl-a in 2020 remained stable at ~0.74 μg L^{-1}, similar to 2018. The $\delta^{13}C_{POC}$ in 2020 followed the same trend as Chl-a, with constant bottom

https://doi.org/10.5194/egusphere-2025-2502
Preprint. Discussion started: 21 July 2025

values (around -26‰) and higher surface values (> -24.5‰).

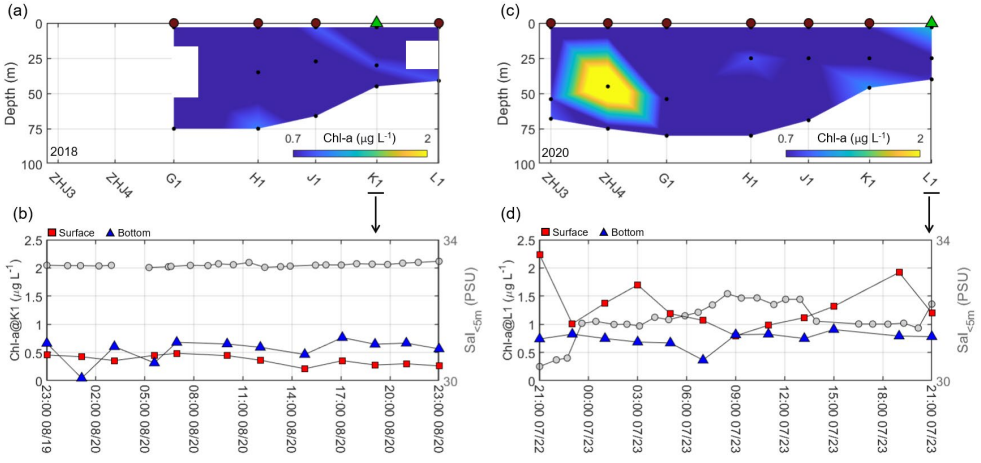

Figure 4: Chl-a measurements along the transect in 2018 (left) and 2020 (right). Brown circles and green triangles denote hydrographic stations (as in Fig. 1), and black dots indicate sampling depths. White areas indicate missing data due to water sample unavailability or technical issues. Time-series data are shown for Station K1 in 2018 (b) and Station L1 in 2020 (d). Red squares and blue triangles represent surface and bottom samples, respectively, while gray dots indicate salinity averaged within 5 m.

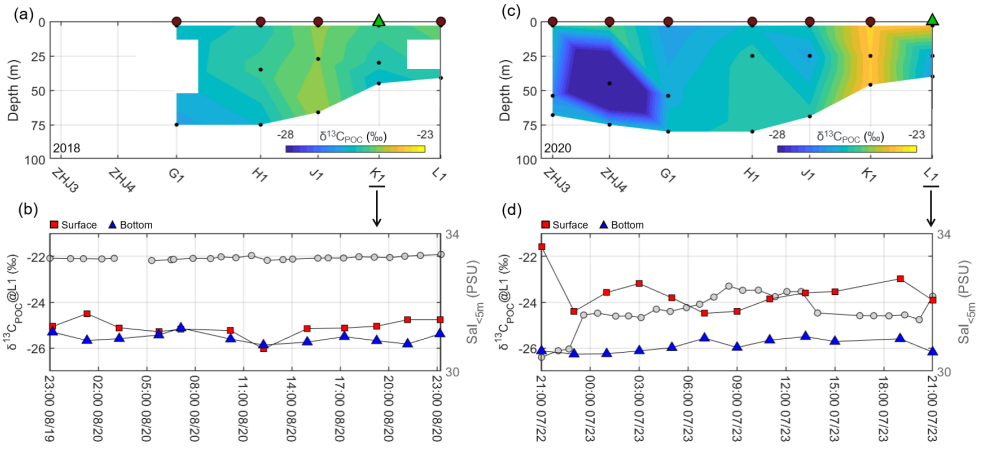

Figure 5: $\delta^{13}C_{POC}$ measurements along the transect in 2018 (left) and 2020 (right). Brown circles and green triangles denote hydrographic stations (as in Fig. 1), with black dots indicating sampling depths. White areas indicate missing data due to water sample unavailability or technical issues. Time-series data are shown for Station K1 in 2018 (b) and Station L1 in 2020 (d). Red squares and blue triangles represent surface and bottom samples,

https://doi.org/10.5194/egusphere-2025-2502
Preprint. Discussion started: 21 July 2025

while gray dots indicate salinity averaged within 5 m.

3.3 Variability in Particle Size and PC Ratios on the NSCS Shelf

Previous studies have documented significant spatial and temporal variability in particle size across the NSCS (Li et al., 2018; Wang et al., 2022), noting that most phytoplankton in the region are smaller than 200 μm (Dong et al., 2018; Liu et al., 2016). Therefore, the LISST measurement threshold of 195 μm was adopted to distinguish biogenic substances from non-biogenic and degraded particles. VC profiling in 2018 indicated that particles were predominantly in the >195 μm size class (Fig. 6a, b), with high values observed at 25 m at Stations G1 and J1, as well as in the bottom water at Station L1. In contrast, VC profiles from 2020 showed distinct distribution patterns across various grain-size classes. High VC measurements for particles <195 μm were recorded at approximately 43 m at Station ZHJ4 and at the surface at Station L1 (Fig. 6c). Conversely, high VC values for the >195 μm size class were found in the middle water column at Stations ZHJ4, G1, and K1, as well as in the surface water at Station L1 (Fig. 6d).

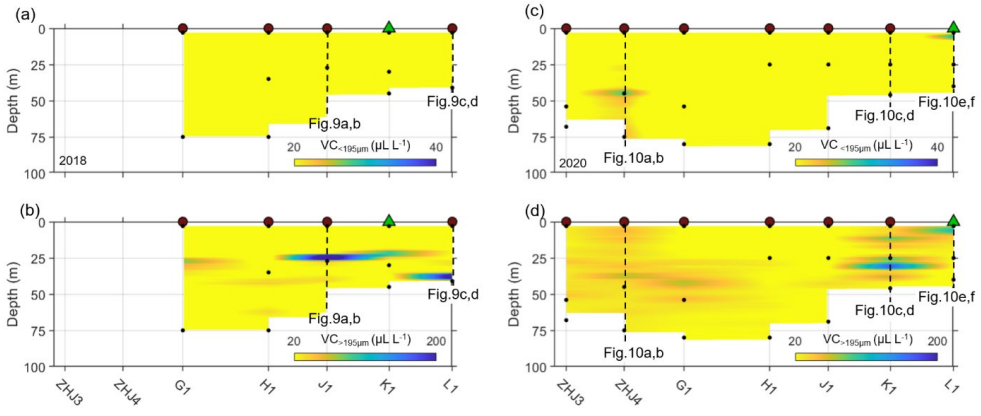

Figure 6: Normalized VC measurements along the transect in 2018 (a, b) and 2020 (c, d). Panels (a, c) display data for particles <195 μm, while (b, d) show data for particles >195 μm. Brown circles and green triangles mark hydrographic stations (as in Fig. 1), with black dots representing sampling depths. Dashed lines indicate VC profiling shown in Figs. 9 and 10.

https://doi.org/10.5194/egusphere-2025-2502
Preprint. Discussion started: 21 July 2025

4. Discussion

4.1 Co-variability among properties of water masses and particles

To better understand the complex interactions among vertical mixing processes, particle sources, and biogeochemical responses in the coastal environment, an empirical orthogonal function (EOF) analysis was conducted to quantify multivariable correlations of these variables on the NSCS shelf. EOF analysis has been widely applied to various river-sea systems (Du et al., 2022; Lee et al., 2016; Liu et al., 2019, 2021; Tao et al., 2022) and upstream regions of the ZRP (Lee et al., 2021, 2023). Based on the EOF eigenvectors of independent variables, the co-variability between intrinsic water properties and the biogeochemical characteristics of transported particles was objectively identified for each eigenmode. The corresponding eigenweightings represent the spatial signatures of these eigenmodes, hierarchically ordered by their corresponding eigenvalues.

This study incorporated three groups of variables in the EOF analysis: (I) salinity, temperature, and the E value, which represent water mass properties and mixing; (II) fluorescence, Chl-a, and $\delta^{13}C_{POC}$, which indicate biogeochemical characteristics of suspended particles; and (III) VC in two size classes (<195 μm and >195 μm), reflecting the physical properties of suspended particles (Fig. 7a-b, Fig. 8a-c). Variables having eigenvector values below 0.1 were considered insignificant. Chl-a and $\delta^{13}C_{POC}$ were excluded from the 2018 EOF analysis due to missing water samples but were included in 2020 to provide a more comprehensive understanding of particle dynamics.

The first two eigenmodes of the 2018 cruise explained nearly 70% of the dataset's variability (Fig. 7a, b), with both modes representing the influence of water stratification. The 1st eigenmode (42.7%; Fig. 7a) showed a negative value for temperature in the eigenvector, while all other variables were positive. This suggests that cold, saline water promoted vertical stability and contained biogeochemical particles of various sizes, as indicated by the positive fluorescence and VCs. In contrast, the 2nd eigenmode (26.4%; Fig. 7b) revealed an inverse

https://doi.org/10.5194/egusphere-2025-2502
Preprint. Discussion started: 21 July 2025

relationship between salinity and the E value, while all other variables had positive in the eigenvector values. This suggests that a diluted water mass (i.e., ZRP) contributed to water stratification and promoted larger suspended particles, as indicated by the strong positive eigenvector for $VC_{>195\mu m}$. The eigenweightings of the first two eigenmodes indicated that distinct water masses occupied different layers of the water column, with the 25-45 m depth range serving as a boundary, as marked by the zero-crossing in the eigenweightings (Fig. 7c-d). The cold seawater represented by the 1st eigenmode was confined to the lower water column (Fig. 7c), where peak positive eigenweightings indicating the accumulation of bio-particle, such as the SCM observed at Station G1. Meanwhile, the diluted plume water represented by the 2nd eigenmode occupied the upper water column (Fig. 7d), influenced by local precipitation (Appendix Fig. A2). Thus, the 2018 EOF analysis highlights how water stability, regulated by the interplay between subsurface seawater and surface-diluted water, shapes the distribution of suspended particles.

Due to weak water stratification along the NSCS shelf in 2020 (Fig. 2g), the EOF analysis yields different results in the first two eigenmodes, which together explained 69.5% of the dataset's co-variability (Fig. 8a-b). The 1st eigenmode (39.1%; Fig. 8a) showed positive eigenvector values for salinity, fluorescence, Chl-a, and $VC_{<195\mu m}$, while the remaining variables were negative. This indicates that cold, saline water was associated with finer biogenic particles and relatively depleted $\delta^{13}C_{POC}$. The eigenweightings were significantly higher in the middle water at Station ZHJ4 (Fig. 8d), reflecting the characteristics of the SCM on the NSCS shelf. The 2nd eigenmode (30.4%; Fig. 8b) showed only salinity as a negative eigenvector, suggesting that a diluted water mass contributed to stratification and entrained biogenic particles with relatively enriched $\delta^{13}C_{POC}$ and a range of particle sizes. The 2nd mode's eigenweightings indicated that diluted water primarily occupied the surface layer at Station L1 (Fig. 8e), consistent with the ZRP pathway observed in 2020. While seawater-induced stratification dominated the 1st eigenmode in 2018, it appeared in the 3rd eigenmode in 2020

https://doi.org/10.5194/egusphere-2025-2502
Preprint. Discussion started: 21 July 2025

(12.7%; Fig. 8c, f), which displayed positive eigenvectors for all variables except temperature and $VC_{<195\mu m}$. This suggests that cold seawater enhanced stability and carried coarser particles with relatively enriched $\delta^{13}C_{POC}$ values to the SCM in the measurement. The 3rd eigenmode's eigenweighting showed a zero-crossing, separating the shelf into upper and lower water columns characterized by distinct water masses and particle properties (Fig. 8f), consistent with the EOF results of the 2018 cruise (Fig. 7c).

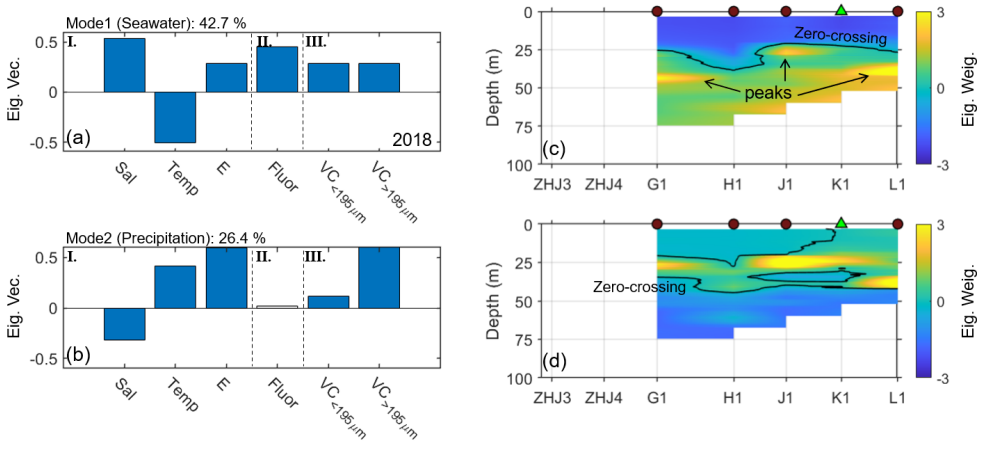

Figure 7: First two modes of the 2018 EOF analysis. The 1st and 2nd modes are shown in the top and bottom panels, respectively. Eigenvectors for each mode are in (a) and (b), while eigenweightings are in (c) and (d). Eigenvalues and corresponding interpretations are listed in the upper left corner of each eigenvector panel. The dashed line categorizes parameters into three groups: (I) water mass properties, (II) biogeochemical features of transported particles, and (III) physical characteristics of suspended particles. Gray bars indicate parameters with eigenvector values <0.1, excluded from EOF interpretation. The black line in the eigenweighting represents the zero-crossing depth. Brown circles and green triangles denote hydrographic sites (as in Fig. 1).

https://doi.org/10.5194/egusphere-2025-2502
Preprint. Discussion started: 21 July 2025

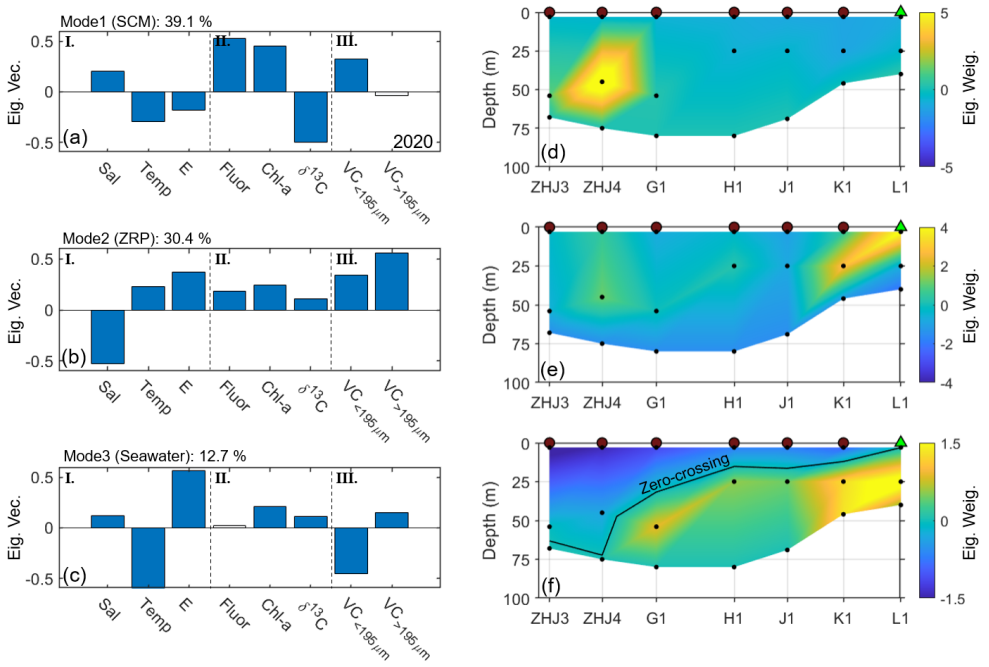

Figure 8: First three modes of the 2020 EOF analysis. The 1st, 2nd, and 3rd modes are shown in the top, middle, and bottom panels, respectively. Eigenvectors for each mode are in (a), (b), and (c), and eigenweightings in (d), (e), and (f). Eigenvalues and interpretations are in the upper left of each eigenvector panel. The dashed line categorizes parameters into three groups: (I) water mass properties, (II) biogeochemical features of transported particles, and (III) physical characteristics of suspended particles. Gray bars indicate parameters with eigenvector values <0.1, excluded from EOF interpretation. The black line in the 3rd mode represents the zero-crossing depth. Brown circles and green triangles denote hydrographic sites (as in Fig. 1).

https://doi.org/10.5194/egusphere-2025-2502
Preprint. Discussion started: 21 July 2025

4.2 Particle distribution associated with water stratification on the NSCS Shelf

Salinity and temperature are key factors influencing water stability in coastal environments, with salinity serving as a primary driver of stratification (Maes et al., 2014). In 2018, stratification was notably enhanced due to the formation of a low-salinity surface layer across the shelf (Fig. 2a, c). Satellite data indicated that increased rainfall led to lower surface salinity in the region (Appendix Fig. A2). In contrast, stratification along the transect in 2020 was relatively weak ($E < 5 \times 10^{-3}$), despite the presence of warm surface water (Fig. 2f, g). Nevertheless, the ZRP transported low-salinity water along its pathway, enhancing stability at the surface of Station L1 (Fig. 2e, g) and causing the halocline to shoal to depths shallower than 25 m.

On the NSCS shelf, water stratification plays a crucial role in regulating the distribution of suspended particles. The highest concentrations of coarse particles (>195 μm) were observed within strongly stratified layers (Figs. 9, 10, and Appendix Figs. A4, A5). This phenomenon, known as the intermediate nepheloid layer (INL; Tian et al., 2022), has been documented in various coastal systems, including the East China Sea shelf (Guo et al., 2010), the Cariaco Basin (Lorenzoni et al., 2009), and the Taiwan Strait (Du and Liu, 2017). The INL can originate either from settling particles within a buoyant river plume (Du and Liu, 2017; Lorenzoni et al., 2009) or from resuspended seafloor sediments driven by high-energy processes, such as nonlinear internal waves (Feng et al., 2021; Lee et al., 2021). Material accumulates at the pycnocline due to strong vertical density gradients, which inhibit mixing caused by surface winds and bottom boundary currents (Du and Liu, 2017; Fortini et al., 2016; Franks, 1992; Lee et al., 2021).

In areas adjacent to the ZRP, such as Station K1, coarse particles were vertically redistributed throughout the water column due to a deeper stratified layer (Fig. 6d and 10c, d). This suggests enhanced vertical transport of particulate matter, and is consistent with the findings that the strength and spatial distribution of plume-induced stratification are key factors

https://doi.org/10.5194/egusphere-2025-2502
Preprint. Discussion started: 21 July 2025

458 in regulating the vertical exchange of marine substances (Cui et al., 2019; Luo et al., 2009).
459 The dispersal of the ZRP on the NSCS shelf is closely tied to river runoff. Although artificial
460 dams along the Zhujiang River regulate outflow at the river mouth, intense precipitation
461 associated with climate variability (e.g., ENSO) has caused flooding in the river basin,
462 potentially reinforcing vertical stability on the continental shelf (Bermúdez et al., 2021; Moser
463 et al., 2012; Peng et al., 2018; Voynova et al., 2012).

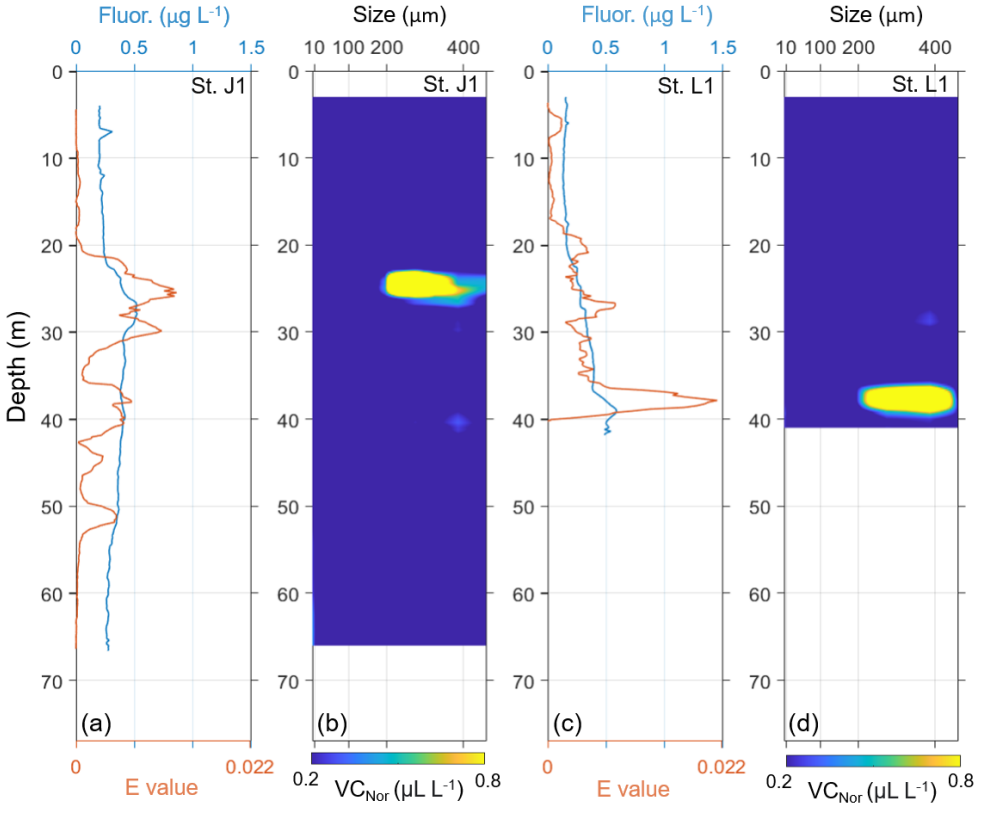

464
465 **Figure 9:** Hydrographic (a, c) and VC (b, d) profiles at Stations J1 and L1 in 2018, as shown
466 in Fig 6. The brown and cyan lines in hydrographic profiles represent the E value and
467 fluorescence, respectively. The grain-size spectrum shows normalized VC.
468

https://doi.org/10.5194/egusphere-2025-2502
Preprint. Discussion started: 21 July 2025

4.3 POM distribution on the NSCS Shelf

The SCM and ZRP were identified on the NSCS shelf based on their physical and biogeochemical characteristics. While both exhibited similar features, such as high Chl-a concentrations (Fig. 4), they differed in $\delta^{13}C_{POC}$ signatures, the VC size composition, PC ratios, and particle bulk density (Fig. 5, 6, Table 2, Appendix Fig. A6). The lower PC ratio and particle bulk density in the SCM suggest the presence of relatively fresher bio-particles compared to those in the ZRP (Appendix Fig. A6). The depleted $\delta^{13}C_{POC}$ in the SCM may result from factors such as phytoplankton size composition and biological metabolism under conditions of low dissolved CO_2 concentration (Close et al., 2020; Law et al., 1995; Liu et al., 2018c; Miller et al., 2008). Although low $\delta^{13}C_{POC}$ values are traditionally considered indicative of terrestrial input (Cai et al., 1988), misidentification of POM sources can occur without multivariable constraints (Lee et al., 2023).

The SCM is typically found near the pycnocline, where nutrient enrichment and optimal light conditions favor phytoplankton growth (Lu et al., 2010). The VC profile (Fig. 10a, b and Appendix Fig. A5) revealed that the SCM was positioned below the pycnocline and primarily composed of finer particles (<10 μm), consistent with previous findings (Chen et al., 2021; Liu et al., 2016; Ning et al., 2004; Williams et al., 2013). However, Xu et al. (2022) reported that in offshore areas deeper than 100 m, the SCM was located above the pycnocline, highlighting the complexity of its distribution in the NSCS.

Previous studies on the upper reaches of the ZRP have shown that most entrained particles in the river plume originate from marine biogenic sources, as substantial terrestrial particles are either trapped upstream by dam operations or rapidly settle upon entering the Zhujiang River Estuary (He et al., 2020; Lee et al., 2023; Wei et al., 2021; Xia et al., 2004). As a result, the low bulk density and enriched $\delta^{13}C_{POC}$ observed along the river plume pathway, particularly at the surface of Station L1 (1288.64 kg m^{-3} in particle bulk density and > -24.5‰ in $\delta^{13}C_{POC}$; Fig. 5c, d and Table 2), reflect the dominance of biogenic sources. Despite both ZRP and SCM

https://doi.org/10.5194/egusphere-2025-2502
Preprint. Discussion started: 21 July 2025

being primarily composed of biogenic particles, distinct physicochemical differences were observed. The high PC ratio in the ZRP suggests that POM was more degraded in the river plume compared to that of the SCM (Table 2; Appendix Fig. A6), resulting to higher particle bulk density (1288.64 kg m^{-3}). Although the PC ratio can be influenced by biological communities (Lee et al., 2020) and the contribution of transparent exopolymer particles (TEPs; Passow, 2002), the low Chl-a concentrations in the ZRP support our interpretation (Fig. 4c). Moreover, strong stratification within the plume suppressed the vertical mixing, allowing degraded particles to remain suspended in the surface layer (Fig. 10e, f).

A bimodal particle size distribution (273 and 386 µm; Fig. 10f) in the ZRP could be attributed to degradation of meso-sized POM (Chen et al., 2015). Additional processes, including zooplankton grazing (Branco et al., 2019; Chen et al., 2015; Landry et al., 1982), bio-aggregation (Mari et al., 2017; Michels et al., 2018), and interactions among various biological communities (Ning et al., 2004; Tong et al., 2023; Zhou et al., 2015), may also potentially contribute to the high VC of particles ranging from 200 to 400 µm at the surface of Station L1.

https://doi.org/10.5194/egusphere-2025-2502
Preprint. Discussion started: 21 July 2025

510 **Table 2:** Derived particle bulk densities (top two tables) and PC ratios (bottom two tables) at
511 each hydrographic site in 2018 and 2020.

2018

Bulk Den. (kg m^{-3})	ZHJ3	ZHJ4	G1	H1	J1	K1	L1
Surface	-	-	-	2715.46	5019.05	2771.29	2229.94
Middle	-	-	-	2735.6	2126.07	2280.33	-
Bottom	-	-	-	**2266.39**	1934.63	1972.99	1905.94

* Bold type indicates Chla >1 µg/L

*"-" symbol indicates missing or error data, and gray value indicates VC <0.1 µL/L or SSC <1 mg/L.

2020

Bulk Den. (kg m^{-3})	ZHJ3	ZHJ4	G1	H1	J1	K1	L1 (ZRP)
Surface	1040.39	1077.85	1047.72	1160.09	1192.47	1447.45	**1288.64**
Middle	1127.11	**1097.2**	1130.36	1192.22	1307.08	1101.51	1496.24
Bottom	1103.01	1139.84	1171.27	1198.12	1302.8	**1199.42**	1655.39

* Bold type indicates Chla >1 µg/L

*"-" symbol indicates missing or error data, and gray value indicates VC <0.1 µL/L or SSC <1 mg/L.

2018

PC Ratio	ZHJ3	ZHJ4	G1	H1	J1	K1	L1
Surface	-	-	579.99	514.81	190.82	673.68	424.27
Middle	-	-	-	558.47	476.45	168.04	-
Bottom	-	-	515.6	**158.07**	470.72	331.98	185.65

* Bold type indicates Chla >1 µg/L

* "-" symbol indicates missing or error data, and gray value indicates POC <0.1 mg/L or Chla <0.5 µg/L

2020

PC Ratio	ZHJ3	ZHJ4	G1	H1	J1	K1	L1 (ZRP)
Surface	363.54	324.57	493.72	235.82	348.42	353.24	**233.19**
Middle	95.63	**52.42**	159.34	112.27	119.15	288.2	275.22
Bottom	103.59	160.17	212.61	834.76	181.14	**163.04**	248.4

* Bold type indicates Chla >1 µg/L

* "-" symbol indicates missing or error data, and gray value indicates POC <0.1 mg/L or Chla <0.5 µg/L

512

https://doi.org/10.5194/egusphere-2025-2502
Preprint. Discussion started: 21 July 2025

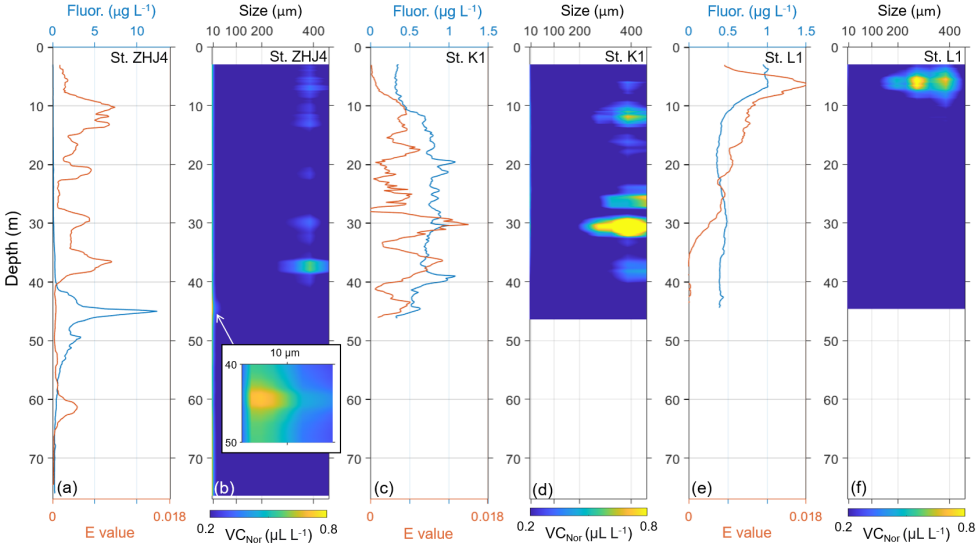

Figure 10: Hydrographic (a, c, e) and normalized VC profiles (b, d, f) at Stations ZHJ4, K1, and L1 in 2020, as shown in Fig 6. The brown and cyan lines in hydrographic profiles represent the E value and fluorescence, respectively. The inset in (b) provides a zoomed-in view of the finer VC size class.

https://doi.org/10.5194/egusphere-2025-2502
Preprint. Discussion started: 21 July 2025

4.4 Implications of biogeochemical signatures in transported particles

Annual sediment transport in the Pearl River Estuary predominantly follows a westward trajectory, leading to significant sediment accumulation toward Hainan Island (Chen, 2006; Gu et al., 2024; Hu et al., 2011; Tian et al., 2019; Wang et al., 2023). However, the eastward-spreading ZRP, driven by the prevailing summer monsoon, offers an alternative pathway for riverine materials to reach the NSCS shelf (Cai et al., 2023; Cao et al., 2019; Jia et al., 2023; Liu et al., 2010). Our findings, consistent with Lee et al. (2023), indicate that particles transported by the northeastward-flowing ZRP are primarily marine-derived biogenic substances (Fig. 2, 4, 5, and Table 2). The presence of marine POM within the river plume suggests a high carbon settling flux in the eastern NSCS shelf (Chen et al., 2022; Hung et al., 2007; Wei et al., 2020), which influences sediment composition along the ZRP pathway (Cai et al., 2023; Chen et al., 2022; Guo et al., 2019) and facilitates material transport toward the Taiwan Strait (Tong et al., 2024).

Our results show an enriched $\delta^{13}C_{POC}$ signature in coastal regions influenced by ZRP, highlighting a clear two-end-member mixing trend between riverine input and ambient seawater (Fig. 11a; Appendix Fig. A7). POM in the proximal ZRP region near Hong Kong (salinity < 30) exhibits a $\delta^{13}C_{POC}$ value of -21.18‰ and a C/N ratio of 7.32 (Lee et al., 2023). In the distal region of the ZRP near offshore Shanwei, $\delta^{13}C_{POC}$ decreases to -23.45‰ with a C/N ratio of 10.25, indicating a progressive dilution with a seawater end-member ($\delta^{13}C_{POC}$ value of -25.4‰ and a C/N ratio of 14.73). Although POM within the ZRP is considered degraded in our study, the $\delta^{13}C_{POC}$ signature remains discernible after extended downstream propagation from the river mouth, highlighting its potential as a tracer of riverine influence over a broad spatial scale. Notably, the $\delta^{13}C_{POC}$ signature of the ZRP also aligns with values observed in the upper 50 m at the SEATS (Southeast Asian Time-series Station; Fig. 11b; Liu et al., 2007). This suggests that stable carbon isotope fractionation follows a similar mechanism in both eutrophic (nearshore) and oligotrophic (offshore) environments, despite differences in

https://doi.org/10.5194/egusphere-2025-2502
Preprint. Discussion started: 21 July 2025

plankton communities across water masses (Ho et al., 2015; Huang et al., 2010; Li et al., 2018, 2021; Lu et al., 2015; Miller et al., 2008; Phillips et al., 2005; Quay et al., 2015; Yin et al., 2001).

Climatic variability could further complicate particle distribution and biogeochemical responses on the NSCS shelf, as rapid fluctuations in river discharge and sediment load from the Zhujiang River impact the system (Liu et al., 2017, 2018a; Xiao et al., 2016; Zhang et al., 2015). Increased flooding events in the river basin may extend the dispersal of terrestrial effluents into the marine environment, blurring the distinction between inshore and offshore waters (Brando et al., 2015; Ren et al., 2020; Shi & Wang, 2009). Physical mechanisms, such as upwelling circulations and nonlinear internal waves (Feng et al., 2021; Gan et al., 2009; Gu et al., 2012; Jing et al., 2009; Lee et al., 2021), further contribute to the mixing of particles from different sources. This process leads to a decoupling of POM signatures between the water column and surface sediments observed in the previous work (Lee et al., 2023). Given these complexities, the multivariable approach applied in this study provides a framework for accurately identifying particle sources and tracking their transport dynamics on the NSCS shelf.

https://doi.org/10.5194/egusphere-2025-2502
Preprint. Discussion started: 21 July 2025

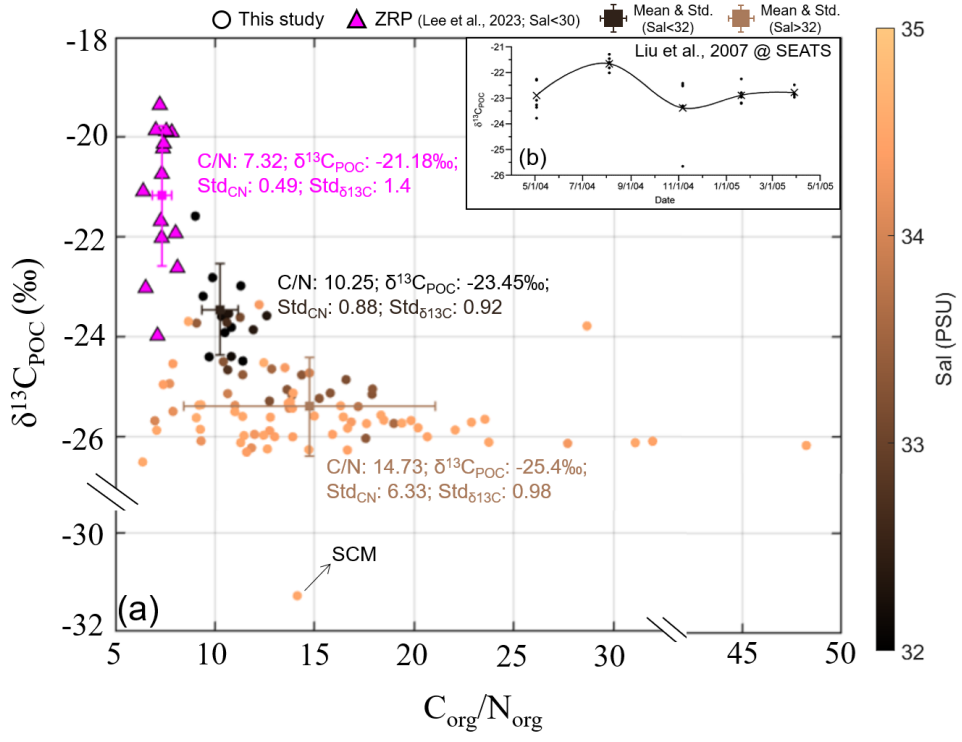

Figure 11: (a) $\delta^{13}C_{POC}$ and C/N ratio results for 2018 and 2020. Circles represent POM samples from this study, colored by corresponding salinity. Magenta triangles denote POM measurements from Lee et al. (2023) for waters with salinities <30. Squares indicate mean $\delta^{13}C_{POC}$ and C/N ratio values, with standard deviations noted beside them. (b) Time-series $\delta^{13}C_{POC}$ observations in the upper 50 m at SEATS from Liu et al. (2007). Cross symbols and a black curve in (b) indicate the mean trend during the observation period, while black dots represent raw data at each sampling.

https://doi.org/10.5194/egusphere-2025-2502
Preprint. Discussion started: 21 July 2025

5. Conclusion

This study underscores the critical role of water stratification in regulating particle distribution on the NSCS shelf, particularly along the northeastward ZRP pathway (Fig. 12). EOF analysis indicates that vertical water stability was shaped by local precipitation, subsurface seawater, and the ZRP, which together governed particle accumulation at the pycnocline. In 2018, strong water stratification induced by precipitation from a tropical depression and subsurface seawater facilitated the retention of larger particles (>195 μm) between 25 and 45 m depth (Fig. 12a, c). In contrast, reduced offshore rainfall in 2020 shifted the dominant stratification mechanism, with ZRP becoming the primary driver under the influence of the southwesterly monsoon. This led to a shoaling of the halocline to depths shallower than 20 meters (Fig. 12b, d), while subsurface seawater continued to contribute to vertical water stability, as indicated by the third mode of the EOF analysis.

Our findings indicate that the ZRP plays a key role in transporting riverine nutrients and marine-sourced biogenic particles toward the Taiwan Strait, potentially shaping sediment composition and coastal biogeochemistry along its pathway. Although both the ZRP and SCM exhibited high Chl-a concentrations, their POM characteristics differed markedly. The ZRP transported more degraded organic material, as reflected by higher PC ratios and greater particle bulk densities, while the SCM was dominated by fresher biogenic particles with lower PC ratios and lighter bulk densities (Fig. 12d). These contrasts underscore distinct particle transport processes, with the ZRP carrying relatively degraded material due to prolonged transit, whereas the SCM reflects *in-situ* phytoplankton production. Furthermore, the distinct $\delta^{13}C_{POC}$ signatures observed among the ZRP, SCM, and ambient seawater highlight its potential as an effective tracer for distinguishing water masses in the NSCS shelf environments. In contrast, the N/P ratio exhibited minimal variability, limiting its effectiveness as a conventional tracer of the ZRP spreading.

https://doi.org/10.5194/egusphere-2025-2502
Preprint. Discussion started: 21 July 2025

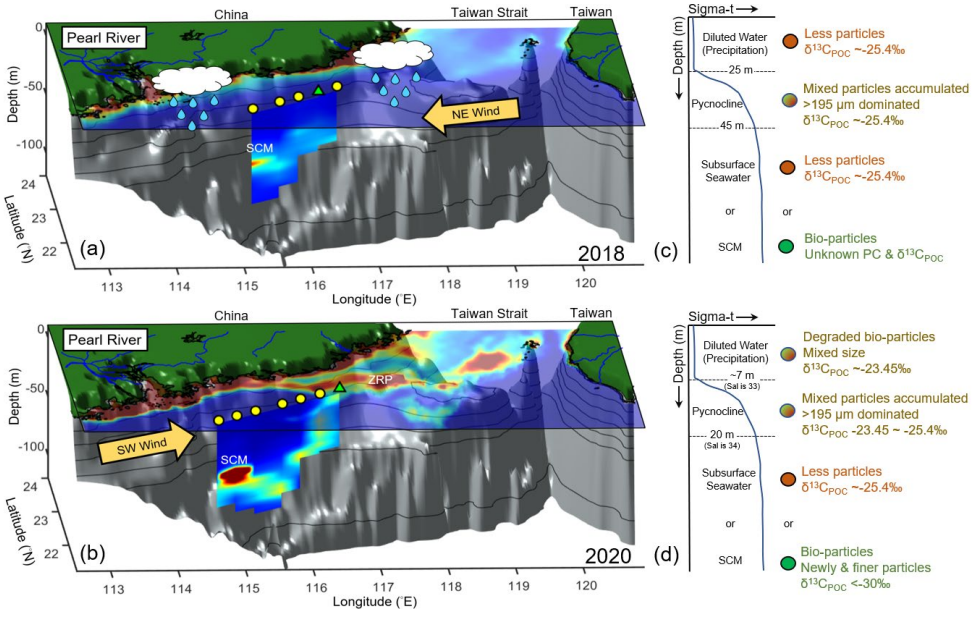

Figure 12: Schematic of particle distribution on the NSCS shelf. Panels (a, b) illustrate two scenarios: local precipitation (2018) and ZRP influence (2020), enhancing vertical water stability. Color images show satellite-derived Chl-a concentrations (horizontal view; same as Fig. 1b, e). Yellow circles and green triangles mark hydrographic sites (as in Fig. 1). Panels (c, d) display corresponding characteristics of suspended particles along the water density profile, linked to water stratification in 2018 and 2020. Circles beside the density profile depict particle signatures at different layers, including diluted water, pycnocline, and subsurface seawater (or SCM).

https://doi.org/10.5194/egusphere-2025-2502
Preprint. Discussion started: 21 July 2025

6. Appendices

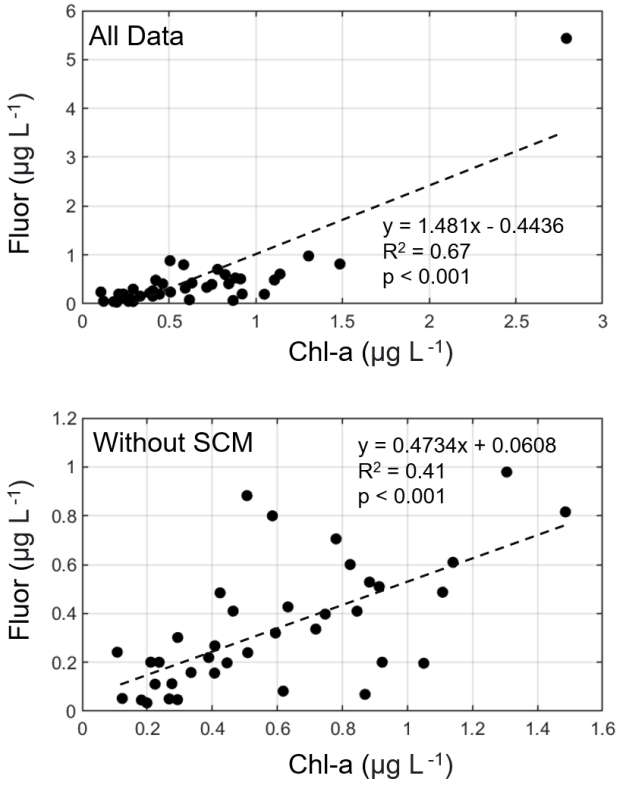

Appendix Fig. A1: Chl-a and fluorescence measurements from 2018 and 2020. The upper panel displays all collected data, while the lower panel excludes data from the SCM. Dashed lines indicate linear regression between Chl-a and fluorescence.

https://doi.org/10.5194/egusphere-2025-2502
Preprint. Discussion started: 21 July 2025

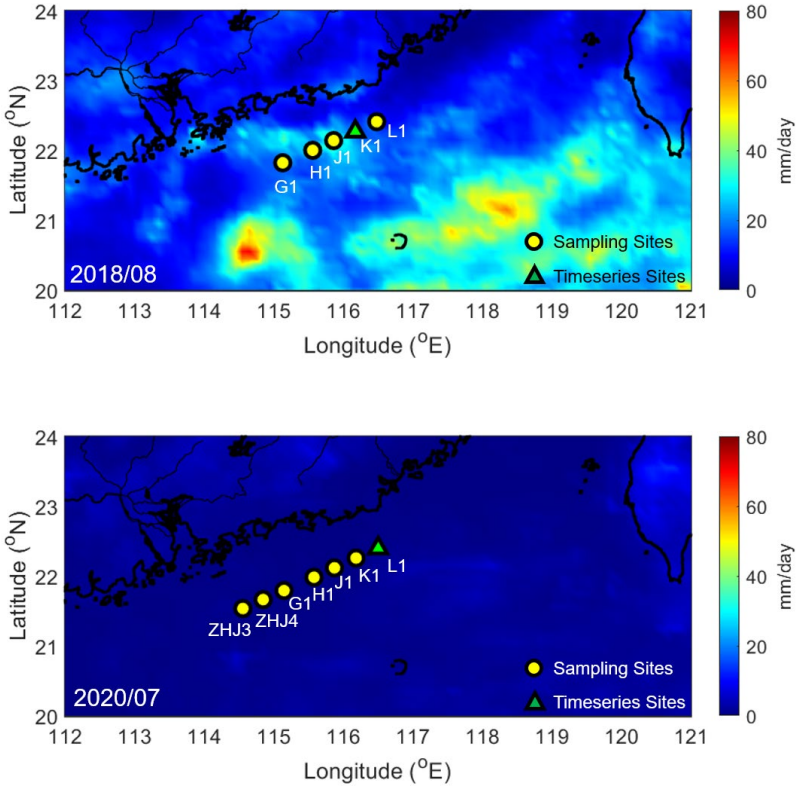

606

607 **Appendix Fig. A2:** Satellite-derived precipitation data during the observation period in 2018
608 (upper panels) and 2020 (lower panels). Yellow circles and green triangles mark hydrographic
609 stations, with green triangles representing time-series stations. Colors indicate precipitation
610 levels obtained from the Integrated Multi-satellite Retrievals for Global Precipitation
611 Measurement (NASA, https://disc.gsfc.nasa.gov/; Huffman et al., 2023).

612

https://doi.org/10.5194/egusphere-2025-2502
Preprint. Discussion started: 21 July 2025

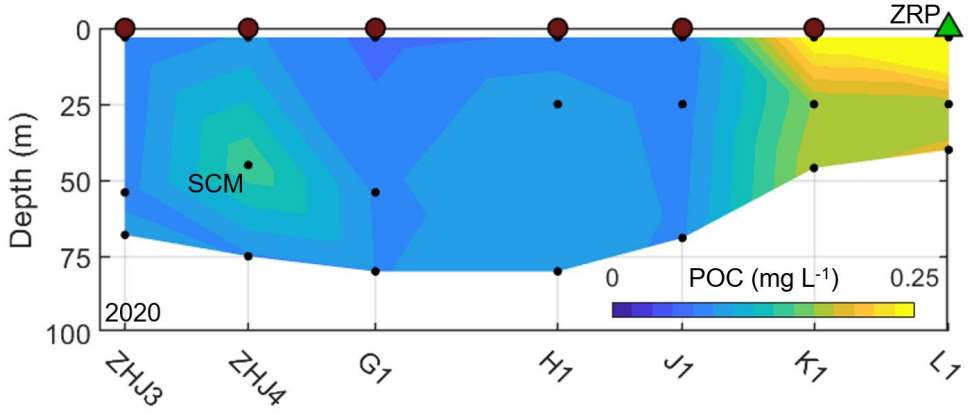

Appendix Fig. A3: POC concentration along the transect in 2020. Black dots indicate sampling depths, while brown circles represent hydrographic stations from the cruise.

https://doi.org/10.5194/egusphere-2025-2502
Preprint. Discussion started: 21 July 2025

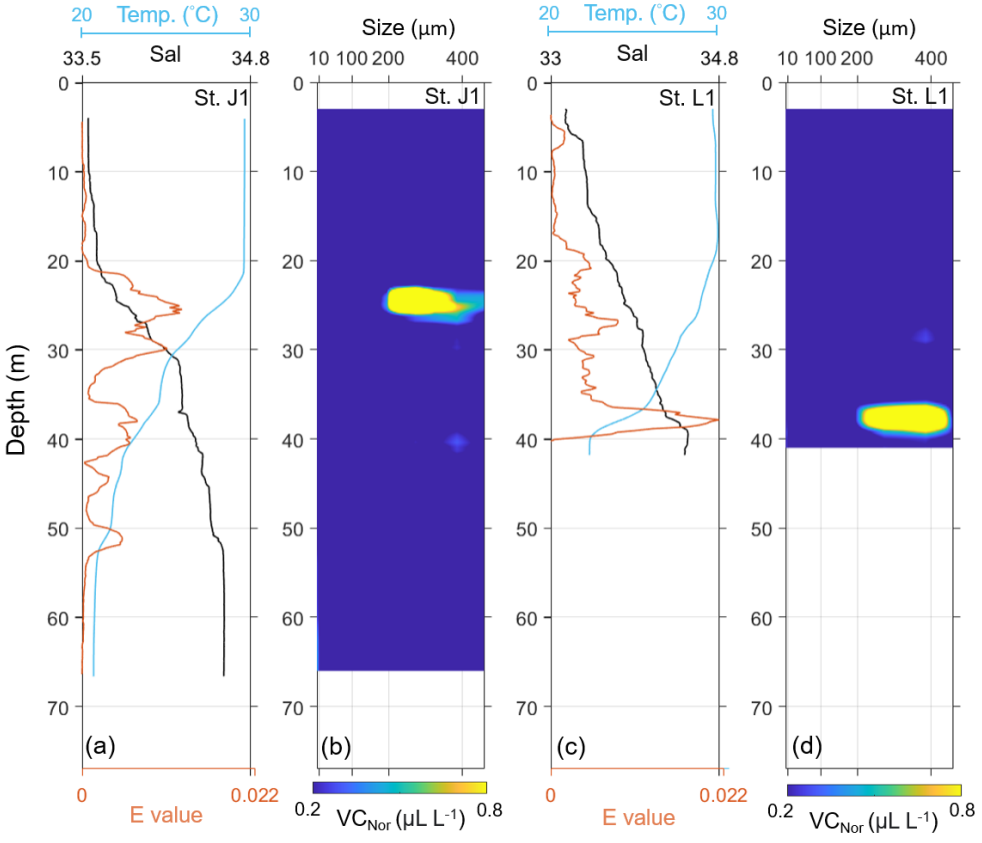

Appendix Fig. A4: Hydrographic (a, c) and VC (b, d) profiles at Stations J1 and L1 in 2018. Black, cyan, and brown lines in the hydrographic profile represent salinity, temperature, and E values, respectively. The spectrum illustrates the normalized volume concentration.

https://doi.org/10.5194/egusphere-2025-2502
Preprint. Discussion started: 21 July 2025

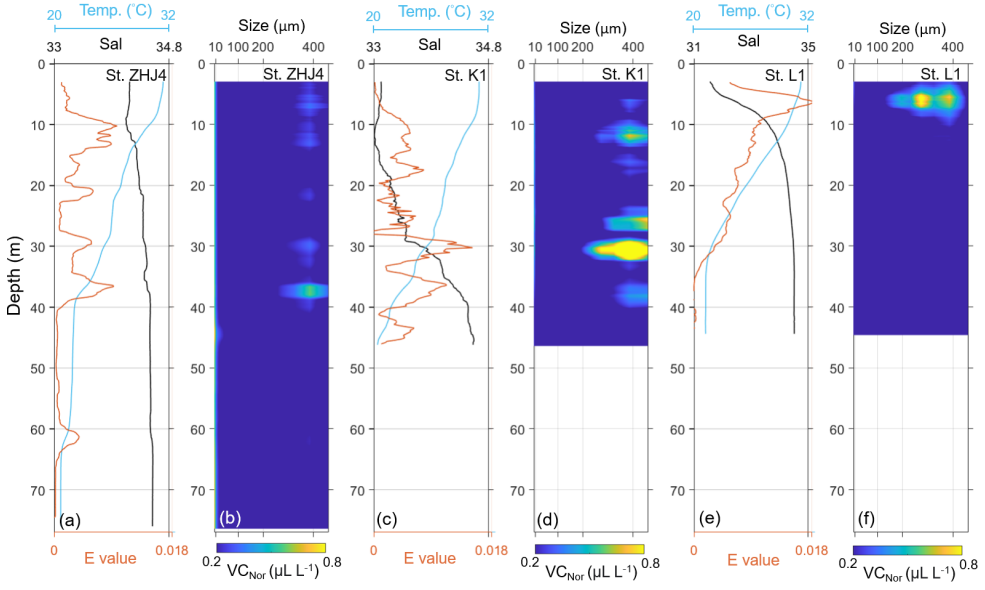

622

623 **Appendix Fig. A5:** Hydrographic (a, c, e) and normalized VC (b, d, f) profiles at Stations ZHJ4,
624 K1, and L1 in 2020 (from left to right). Black, cyan, and brown lines in the hydrographic
625 profiles represent salinity, temperature, and E values, respectively.

626

https://doi.org/10.5194/egusphere-2025-2502
Preprint. Discussion started: 21 July 2025

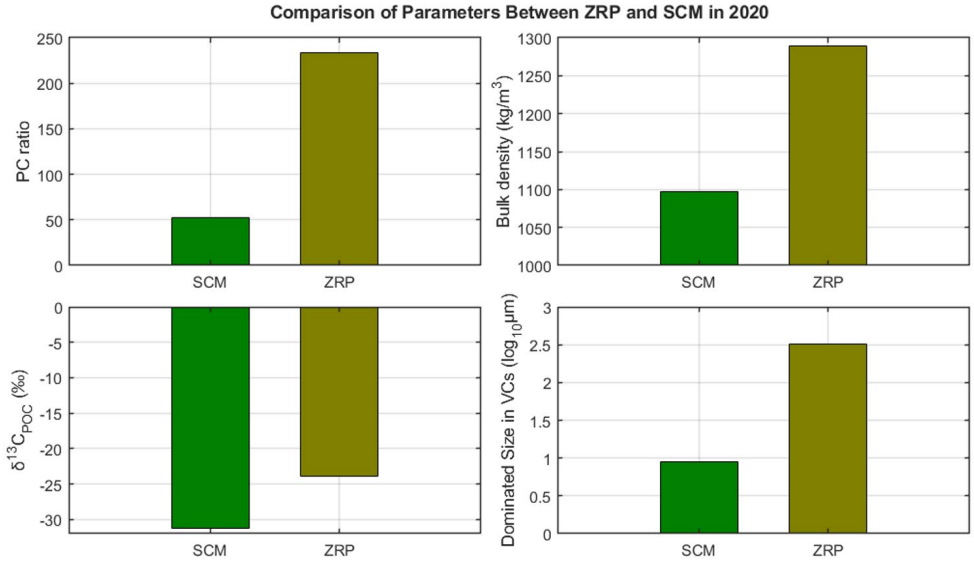

627

628 **Appendix Fig. A6:** Physicochemical characteristics of POM measured in 2020, including the
629 PC ratio, $\delta^{13}C_{POC}$, particle bulk density, and dominant particle size based on VC measurement.
630 The bar chart shows the SCM in green and the ZRP in olive green

https://doi.org/10.5194/egusphere-2025-2502
Preprint. Discussion started: 21 July 2025

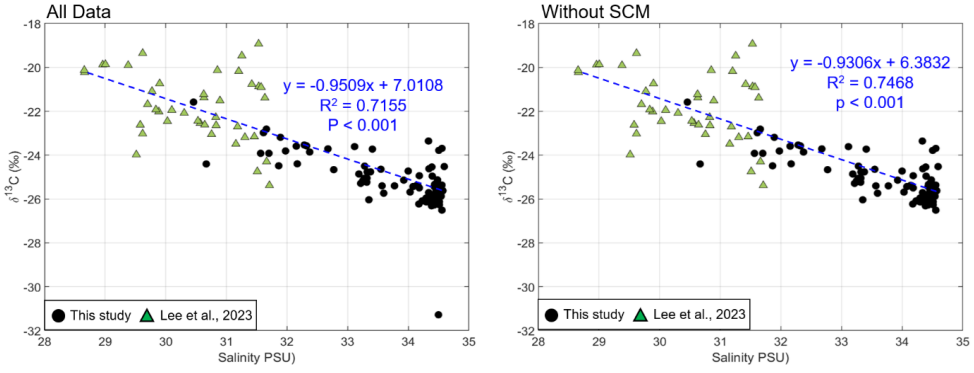

631

632 **Appendix Fig. A7:** Salinity and $\delta^{13}C_{POC}$ measurements from 2018 and 2020. The left panel
633 presents all collected data, while the right panel excludes the SCM. Blue dashed lines indicate
634 linear regression between salinity and $\delta^{13}C_{POC}$.

635

https://doi.org/10.5194/egusphere-2025-2502
Preprint. Discussion started: 21 July 2025

7. Code availability

The code used in this study are available from the corresponding author on reasonable request.

https://doi.org/10.5194/egusphere-2025-2502
Preprint. Discussion started: 21 July 2025

8. Data availability

The datasets used and analyzed in this study are available from the corresponding author on reasonable request.

https://doi.org/10.5194/egusphere-2025-2502
Preprint. Discussion started: 21 July 2025

9. Author Contributions

JL and JTL designed the field observations, with contributions from YSL. Sample analyses were primarily supported by YSL, TYH, and CTAC. WG provided the data resources of the Zhujiang River. JL prepared the initial draft of the manuscript under the supervision of JTL. CRW contributed to manuscript revision. All authors contributed to data interpretation and final manuscript editing.

https://doi.org/10.5194/egusphere-2025-2502
Preprint. Discussion started: 21 July 2025

10. Competing interests

The authors declare that they have no conflict of interest.

https://doi.org/10.5194/egusphere-2025-2502
Preprint. Discussion started: 21 July 2025

11. Acknowledgements

This study was funded by the ROC Ministry of Science and Technology (MOST) under grant numbers MOST 104-2611-M-110-011, MOST 105-2611-M-110-001, MOST 106-2611-M-110-005, and MOST 110-2611-M-110-021. We acknowledge the use of imagery from NASA's Worldview application (https://worldview.earthdata.nasa.gov), part of the Earth Observing System Data and Information System (EOSDIS). We thank the captain and crew of R/V Ocean Researcher III and R/V Legend for their assistance in the fieldwork. We also thank M.-C. Lu and Y.-L. Chou of T.-Y. Ho's team at the Research Center for Environmental Changes, Academia Sinica, the staff and students of C.-T. Arthur Chen's team in the Department of Oceanography at National Sun Yat-sen University, and the Taiwan Ocean Research Institute team for their help with nutrient analyses. During the preparation of this work the author(s) used CGPT in order to improve language and readability, with caution. After using this tool/service, the author(s) reviewed and edited the content as needed and take(s) full responsibility for the content of the publication.

https://doi.org/10.5194/egusphere-2025-2502
Preprint. Discussion started: 21 July 2025

12. References

1. Alford, M. H., Peacock, T., MacKinnon, J. A., Nash, J. D., Buijsman, M. C., Centurioni, L. R., Chao, S.-Y., Chang, M.H., Farmer, D.M., Fringer, O.B., Fu, K.H., Gallacher, P.C., Graber, H.C., Helfrich, K.R., Jachec, S.M., Jackson, C.R., Klymak, J.M., Ko, D.S., Jan, S., Johnston, T.M., Legg, S., Lee, I.H., Lien, R.C., Mercier, M.J., Moum, J.N., Musgrave, R., Park, J.H., Pickering, A.I., Pinkel, R., Rainville, L., Ramp, S.R., Rudnick, D.L., Sarkar, S., Scotti, A., Simmons, H.L., St Laurent, L.C., Venayagamoorthy, S.K., Wang, Y.H., Wang, J., Yang, Y.J., Paluszkiewicz, T., Tang, T.Y. (2015). The formation and fate of internal waves in the South China Sea. *Nature, 521*(7550), 65–69. https://doi.org/10.1038/nature14399

2. Allen, P.A. (2017). Sediment Routing Systems: The Fate of Sediment from Source to Sink. Cambridge University Press, Cambridge. https://doi.org/10.1017/9781316135754

3. Bai, Y., Huang, T.-H., He, X., Wang, S.-L., Hsin, Y.-C., Wu, C.-R., Zhai, W., Lui, H.-K., & Chen, C.-T. A. (2015). Intrusion of the Pearl River plume into the main channel of the Taiwan Strait in summer. *Journal of Sea Research, 95*, 1–15. https://doi.org/10.1016/j.seares.2014.10.003

4. Bermúdez, M., Farfán, J. F., Willems, P., & Cea, L. (2021). Assessing the effects of climate change on compound flooding in coastal river areas. *Water Resources Research, 57*(10), e2020WR029321. https://doi.org/10.1029/2020WR029321

5. Bouillon, S., Connolly, R. M., & Gillikin, D. P. (2011). Use of stable isotopes to understand food webs and ecosystem functioning in estuaries. In Wolanski, E., & McLusky, D. (Eds.), *Treatise on Estuarine and Coastal Science* (pp. 143–173). Waltham: Academic Press. https://doi.org/10.1016/B978-0-12-374711-2.00711-7

6. Bouillon, S., Dehairs, F., Velimirov, B., Abril, G., & Borges, A. V. (2007). Dynamics of organic and inorganic carbon across contiguous mangrove and seagrass systems (Gazi Bay, Kenya). *Journal of Geophysical Research: Biogeosciences, 112*(G2). https://doi.org/10.1029/2006JG000325

7. Boyer, T., Levitus, S., Garcia, H., Locarnini, R. A., Stephens, C., & Antonov, J. (2005). Objective analyses of annual, seasonal, and monthly temperature and salinity for the world ocean on a 0.25° grid. *International Journal of Climatology, 25*(7), 931–945. https://doi.org/10.1002/joc.1173

8. Branco, P., Egas, M., Hall, S. R., & Huisman, J. (2019). Why do phytoplankton evolve large size in response to grazing? *The American Naturalist, 195*(1), E20–E37. https://doi.org/10.1086/706251

https://doi.org/10.5194/egusphere-2025-2502
Preprint. Discussion started: 21 July 2025

9. Brando, V. E., Braga, F., Zaggia, L., Giardino, C., Bresciani, M., Matta, E., Bellafiore, D., et al. (2015). High-resolution satellite turbidity and sea surface temperature observations of river plume interactions during a significant flood event. *Ocean Science, 11*(6), 909–920. https://doi.org/10.5194/os-11-909-2015

10. Cai, D.-L., Tan, F. C., & Edmond, J. M. (1988). Sources and transport of particulate organic carbon in the Amazon River and estuary. *Estuarine, Coastal and Shelf Science, 26*(1), 1–14. https://doi.org/10.1016/0272-7714(88)90008-X

11. Cai, P., Cai, G., Yang, J., Li, X., Lin, J., Li, S., & Zhao, L. (2023). Distribution, risk assessment, and quantitative source apportionment of heavy metals in surface sediments from the shelf of the northern South China Sea. *Marine Pollution Bulletin, 187*, 114589. https://doi.org/10.1016/j.marpolbul.2023.114589

12. Cai, W.-J., Dai, M., Wang, Y., Zhai, W., Huang, T., Chen, S., Zhang, F., Chen, Z., & Wang, Z. (2004). The biogeochemistry of inorganic carbon and nutrients in the Pearl River Estuary and the adjacent northern South China Sea. *Continental Shelf Research, 24*(12), 1301–1319. https://doi.org/10.1016/j.csr.2004.04.005

13. Cao, L., Liu, J., Shi, X., He, W., & Chen, Z. (2019). Source-to-sink processes of fluvial sediments in the northern South China Sea: Constraints from river sediments in the coastal region of South China. *Journal of Asian Earth Sciences, 185*, 104020. https://doi.org/10.1016/j.jseaes.2019.104020

14. Cao, Z., Dai, M., Zheng, N., Wang, D., Li, Q., Zhai, W., Meng, F., & Gan, J. (2011). Dynamics of the carbonate system in a large continental shelf system under the influence of both a river plume and coastal upwelling. *Journal of Geophysical Research: Biogeosciences, 116*(G2). https://doi.org/10.1029/2010JG001596

15. Cathalot, C., Rabouille, C., Tisnérat-Laborde, N., Toussaint, F., Kerhervé, P., Buscail, R., Loftis, K., et al. (2013). The fate of river organic carbon in coastal areas: A study in the Rhône River Delta using multiple isotopic (Δ13C, Δ14C) and organic tracers. *Geochimica et Cosmochimica Acta, 118*, 33–55. https://doi.org/10.1016/j.gca.2013.05.001

16. Chen, D. (2006). The seasonal variation characteristics of residual currents in the Qiongzhou Strait (in Chinese with English abstract). *Transactions of Oceanology and Limnology, 2*(108), 12.

17. Chen, L., Yin, Z., Tang, M., Li, T., & Xu, D. (2022). Distribution and genesis of organic carbon storage on the northern shelf of the South China Sea. *International Journal of*

https://doi.org/10.5194/egusphere-2025-2502
Preprint. Discussion started: 21 July 2025

Environmental Research and Public Health, 19(18). https://doi.org/10.3390/ijerph191811367

18. Chen, M., Liu, H., Song, S., & Sun, J. (2015). Size-fractionated mesozooplankton biomass and grazing impact on phytoplankton in the northern South China Sea during four seasons. *Deep-Sea Research Part II: Topical Studies in Oceanography, 117*, 108–118. https://doi.org/10.1016/j.dsr2.2015.02.026

19. Chen, Y., & Zhao, H. (2021). Spatial distribution of the summer subsurface chlorophyll maximum in the North South China Sea. *PLOS ONE, 16*(4), e0248715. https://doi.org/10.1371/journal.pone.0248715

20. Chen, Y.-L. L., Chen, H.-Y., Karl, D. M., & Takahashi, M. (2004). Nitrogen modulates phytoplankton growth in spring in the South China Sea. *Continental Shelf Research, 24*(4), 527–541. https://doi.org/10.1016/j.csr.2003.12.006

21. Chen, Z., Gong, W., Cai, H., Chen, Y., & Zhang, H. (2017a). Dispersal of the Pearl River plume over the continental shelf in summer. *Estuarine, Coastal and Shelf Science, 194*, 252–262. https://doi.org/10.1016/j.ecss.2017.06.025

22. Chen, Z., Pan, J., & Jiang, Y. (2016). Role of pulsed winds on detachment of low salinity water from the Pearl River plume: Upwelling and mixing processes. *Journal of Geophysical Research: Oceans, 121*(4), 2769–2788. https://doi.org/10.1002/2015JC011337

23. Chen, Z., Pan, J., Jiang, Y., & Lin, H. (2017b). Far-reaching transport of Pearl River plume water by upwelling jet in the northeastern South China Sea. *Journal of Marine Systems, 173*, 60–69. https://doi.org/10.1016/j.jmarsys.2017.04.008

24. Close, H. G., & Henderson, L. C. (2020). Open-ocean minima in Δ13C values of particulate organic carbon in the lower euphotic zone. *Frontiers in Marine Science, 7*. https://www.frontiersin.org/journals/marine-science/articles/10.3389/fmars.2020.540165

25. Cross, J., Nimmo-Smith, W. A. M., Hosegood, P. J., & Torres, R. (2014). The dispersal of phytoplankton populations by enhanced turbulent mixing in a shallow coastal sea. *Journal of Marine Systems, 136*, 55–64. https://doi.org/10.1016/j.jmarsys.2014.03.009

26. Cui, Y., Wu, J., Ren, J., & Xu, J. (2019). Physical dynamic structures and oxygen budget of summer hypoxia in the Pearl River Estuary. *Limnology and Oceanography, 64*(1), 131–148. https://doi.org/10.1002/lno.11025

https://doi.org/10.5194/egusphere-2025-2502
Preprint. Discussion started: 21 July 2025

27. Deuser, W. G. (1970). Isotopic evidence for diminishing supply of available carbon during diatom bloom in the Black Sea. *Nature*, 225, 1069–1071. https://doi.org/10.1038/2251069a0

28. Dong, L., Su, J., Wong, L. A., Cao, Z., & Chen, J.-C. (2004). Seasonal variation and dynamics of the Pearl River plume. *Continental Shelf Research, 24*(16), 1761–1777. https://doi.org/10.1016/j.csr.2004.06.006

29. Dong, Y., Li, Q. P., Liu, Z., Wu, Z., & Zhou, W. (2018). Size-dependent phytoplankton growth and grazing in the northern South China Sea. *Marine Ecology Progress Series, 599*, 35–47. https://www.int-res.com/abstracts/meps/v599/p35-47/

30. Du, X., & Liu, J. T. (2017). Particle dynamics of the surface, intermediate, and benthic nepheloid layers under contrasting conditions of summer monsoon and typhoon winds on the boundary between the Taiwan Strait and East China Sea. *Progress in Oceanography, 156*, 130–144. https://doi.org/10.1016/j.pocean.2017.06.009

31. Du, X., Liu, J. T., Lee, J., Huang, P. S., Yang, R. J., & Jue, P. Z. (2022). Influence of sediment sources, water mass, and physical processes on the dynamics of flocs at a location between the mouth of a river and the head of a submarine canyon. *Marine Geology, 445*, 106736. https://doi.org/10.1016/j.margeo.2022.106736

32. Eisma, D. (1986). Flocculation and de-flocculation of suspended matter in estuaries. *Netherlands Journal of Sea Research, 20*(2), 183–199. https://doi.org/10.1016/0077-7579(86)90041-4

33. Fanning, K. A., & Pilson, M. (1973). On the spectrophotometric determination of dissolved silica in natural waters. *Analytical Chemistry, 45*(1), 136–140. https://doi.org/10.1021/ac60323a021

34. Feng, Y., Tang, Q., Li, J., Sun, J., & Zhan, W. (2021). Internal solitary waves observed on the continental shelf in the northern South China Sea from acoustic backscatter data. *Frontiers in Marine Science, 8*. https://doi.org/10.3389/fmars.2021.734075

35. Fischer, G. (1991). Stable carbon isotope ratios of plankton carbon and sinking organic matter from the Atlantic sector of the Southern Ocean. *Marine Chemistry, 35*(1), 581–596. https://doi.org/10.1016/S0304-4203(09)90044-5

36. Fortini, A., Martín-Fabiani, I., Lesage De La Haye, J., Dugas, P.-Y., Lansalot, M., D'Agosto, F., Bourgeat-Lami, E., Keddie, J. L., & Sear, R. P. (2016). Dynamic stratification in drying films of colloidal mixtures. *Physical Review Letters, 116*(11), 118301. https://doi.org/10.1103/PhysRevLett.116.118301

https://doi.org/10.5194/egusphere-2025-2502
Preprint. Discussion started: 21 July 2025

37. Franks, P. J. S. (1992). Sink or swim: Accumulation of biomass at fronts. *Marine Ecology Progress Series, 82*, 1–12. https://doi.org/10.3354/meps082001

38. Gan, J., Kung, H., Cai, Z., Liu, Z., Hui, C., & Li, J. (2022). Hotspots of the Stokes rotating circulation in a large marginal sea. *Nature Communications, 13*(1), 2223. https://doi.org/10.1038/s41467-022-29610-z

39. Gan, J., Li, L., Wang, D., & Guo, X. (2009). Interaction of a river plume with coastal upwelling in the northeastern South China Sea. *Continental Shelf Research, 29*(4), 728–740. https://doi.org/10.1016/j.csr.2008.12.002

40. Gu, B. (2009). Variations and controls of nitrogen stable isotopes in particulate organic matter of lakes. *Oecologia, 160*(3), 421–431. https://doi.org/10.1007/s00442-009-1323-z

41. Gu, J., Zhang, Y., Tuo, P., Hu, Z., Chen, S., & Hu, J. (2024). Surface floating objects moving from the Pearl River Estuary to Hainan Island: An observational and model study. *Journal of Marine Systems, 241*, 103917. https://doi.org/10.1016/j.jmarsys.2023.103917

42. Gu, X., Zhang, Q., Singh, V. P., & Shi, P. (2017). Hydrological response to large-scale climate variability across the Pearl River Basin, China: Spatiotemporal patterns and sensitivity. *Global and Planetary Change, 149*, 1–13. https://doi.org/10.1016/j.gloplacha.2016.12.016

43. Gu, Y., Pan, J., & Lin, H. (2012). Remote sensing observation and numerical modeling of an upwelling jet in Guangdong coastal water. *Journal of Geophysical Research: Oceans, 117*(C8). https://doi.org/10.1029/2012JC007922

44. Guo, C., & Chen, X. (2014). A review of internal solitary wave dynamics in the northern South China Sea. *Progress in Oceanography, 121*, 7–23. https://doi.org/10.1016/j.pocean.2013.04.002

45. Guo, W., Jia, G., Ye, F., Xiao, H., & Zhang, Z. (2019). Lipid biomarkers in suspended particulate matter and surface sediments in the Pearl River Estuary, a subtropical estuary in southern China. *Science of The Total Environment, 646*, 416–426. https://doi.org/10.1016/j.scitotenv.2018.07.159

46. Guo, W., Ye, F., Xu, S., & Jia, G. (2015). Seasonal variation in sources and processing of particulate organic carbon in the Pearl River Estuary, South China. *Estuarine, Coastal and Shelf Science, 167*, 540–548. https://doi.org/10.1016/j.ecss.2015.11.004

47. Guo, X., Cai, W.-J., Zhai, W., Dai, M., Wang, Y., & Chen, B. (2008). Seasonal variations in the inorganic carbon system in the Pearl River (Zhujiang) Estuary.

https://doi.org/10.5194/egusphere-2025-2502
Preprint. Discussion started: 21 July 2025

Continental Shelf Research, 28(12), 1424–1434. https://doi.org/10.1016/j.csr.2007.07.011

48. Guo, X., Zhang, Y., Zhang, F., & Cao, Q. (2010). Characteristics and flux of settling particulate matter in neritic waters: The Southern Yellow Sea and the East China Sea. *Deep-Sea Research Part II: Topical Studies in Oceanography, 57*(11–12), 1058–1063. https://doi.org/10.1016/j.dsr2.2010.02.007

49. Harrison, P. J., Yin, K., Lee, J. H. W., Gan, J., & Liu, H. (2008). Physical–biological coupling in the Pearl River Estuary. *Continental Shelf Research, 28*(12), 1405–1415. https://doi.org/10.1016/j.csr.2007.02.011

50. He, Z., Jia, L., Jia, Y., & He, J. (2020). Effects of flood events on sediment transport and deposition in the waterways of Lingding Bay, Pearl River Delta, China. *Ocean & Coastal Management, 185*, 105062. https://doi.org/10.1016/j.ocecoaman.2019.105062

51. Hill, P. S., Milligan, T. G., & Geyer, W. R. (2000). Controls on effective settling velocity of suspended sediment in the Eel River flood plume. *Continental Shelf Research, 20*(16), 2095–2111. https://doi.org/10.1016/S0278-4343(00)00064-9

52. Ho, T.-Y., Pan, X., Yang, H.-H., Wong, G. T. F., & Shiah, F.-K. (2015). Controls on temporal and spatial variations of phytoplankton pigment distribution in the northern South China Sea. *Deep-Sea Research Part II: Topical Studies in Oceanography, 117*, 65–85. https://doi.org/10.1016/j.dsr2.2015.05.015

53. Hong, B., Wang, G., Xu, H., & Wang, D. (2020). Study on the transport of terrestrial dissolved substances in the Pearl River Estuary using passive tracers. *Water, 12*(5), 1235. https://doi.org/10.3390/w12051235

54. Horner-Devine, A. R., Hetland, R. D., & MacDonald, D. G. (2015). Mixing and transport in coastal river plumes. *Annual Review of Fluid Mechanics*. Annual Reviews Inc. https://doi.org/10.1146/annurev-fluid-010313-141408

55. Hsu, R. T., & Liu, J. T. (2010). In-situ estimations of the density and porosity of flocs of varying sizes in a submarine canyon. *Marine Geology, 276*(1), 105–109. https://doi.org/10.1016/j.margeo.2010.07.003

56. Hu, J., Li, S., & Geng, B. (2011). Modeling the mass flux budgets of water and suspended sediments for the river network and estuary in the Pearl River Delta, China. *Journal of Marine Systems, 88*(2), 252–266. https://doi.org/10.1016/j.jmarsys.2011.05.002

https://doi.org/10.5194/egusphere-2025-2502
Preprint. Discussion started: 21 July 2025

57. Huang, B., Hu, J., Xu, H., Cao, Z., & Wang, D. (2010). Phytoplankton community at warm eddies in the northern South China Sea in winter 2003/2004. *Deep-Sea Research Part II: Topical Studies in Oceanography, 57*(19), 1792–1798. https://doi.org/10.1016/j.dsr2.2010.04.005

58. Huang, C., Lao, Q., Chen, F., Zhang, S., Chen, C., Bian, P., & Zhu, Q. (2021). Distribution and sources of particulate organic matter in the northern South China Sea: Implications of human activity. *Journal of Ocean University of China, 20*(5), 1136–1146. https://doi.org/10.1007/s11802-021-4807-z

59. Huang, W.-J., Kao, K.-J., Lin, Y.-S., Chen, C.-T. A., & Liu, J. T. (2020). Daily to weekly impacts of mixing and biological activity on carbonate dynamics in a large river-dominated shelf. *Estuarine, Coastal and Shelf Science, 245*, 106914. https://doi.org/10.1016/j.ecss.2020.106914

60. Huffman, G. J., Stocker, E. F., Bolvin, D. T., Nelkin, E. J., & Tan, J. (2023). GPM IMERG Final Precipitation L3 1 Day 0.1 Degree x 0.1 Degree V07. In A. Savtchenko (Ed.), *Goddard Earth Sciences Data and Information Services Center (GES DISC)*. https://doi.org/10.5067/GPM/IMERGDF/DAY/07

61. Hung, J.-J., Wang, S.-M., & Chen, Y.-L. (2007). Biogeochemical controls on distributions and fluxes of dissolved and particulate organic carbon in the northern South China Sea. *Deep-Sea Research Part II: Topical Studies in Oceanography, 54*(14), 1486–1503. https://doi.org/10.1016/j.dsr2.2007.05.006

62. Jago, C. F., Jones, S. E., Sykes, P., & Rippeth, T. (2006). Temporal variation of suspended particulate matter and turbulence in a high-energy, tide-stirred, coastal sea: Relative contributions of resuspension and disaggregation. *Continental Shelf Research, 26*(17), 2019–2028. https://doi.org/10.1016/j.csr.2006.07.009

63. Jakobsen, H. H., & Markager, S. (2016). Carbon-to-chlorophyll ratio for phytoplankton in temperate coastal waters: Seasonal patterns and relationship to nutrients. *Limnology and Oceanography, 61*(5), 1853–1868. https://doi.org/10.1002/lno.10338

64. Jia, J., Wang, C., Su, M., Yan, W., Zeng, L., & Cui, H. (2023). Provenance and dispersal patterns of sediments on the continental shelf of northern South China Sea: Evidence from detrital zircon geochronology. *Marine Geology, 457*, 107013. https://doi.org/10.1016/j.margeo.2023.107013

65. Jiang, Z.-Y., Wang, Y.-S., Cheng, H., Sun, C.-C., & Wu, M.-L. (2015). Variation of phytoplankton community structure from the Pearl River Estuary to South China Sea. *Ecotoxicology, 24*(7), 1442–1449. https://doi.org/10.1007/s10646-015-1494-9

https://doi.org/10.5194/egusphere-2025-2502
Preprint. Discussion started: 21 July 2025

66. Jing, Z.-Y., Qi, Y.-Q., Hua, Z.-L., & Zhang, H. (2009). Numerical study on the summer upwelling system in the northern continental shelf of the South China Sea. *Continental Shelf Research, 29*(2), 467–478. https://doi.org/10.1016/j.csr.2008.11.008

67. Jouon, A., Ouillon, S., Douillet, P., Lefebvre, J. P., Fernandez, J. M., Mari, X., & Froidefond, J.-M. (2008). Spatio-temporal variability in suspended particulate matter concentration and the role of aggregation on size distribution in a coral reef lagoon. *Marine Geology, 256*(1), 36–48. https://doi.org/10.1016/j.margeo.2008.09.008

68. Lan, W., Huang, B., Dai, M., Ning, X., Huang, L., & Hong, H. (2009). Dynamics of heterotrophic dinoflagellates off the Pearl River Estuary, northern South China Sea. *Estuarine, Coastal and Shelf Science, 85*(3), 422–430. https://doi.org/10.1016/j.ecss.2009.09.008

69. Landry, M. R., & Hassett, R. P. (1982). Estimating the grazing impact of marine micro-zooplankton. *Marine Biology, 67*(3), 283–288. https://doi.org/10.1007/BF00397668

70. Laws, E.A., Popp, B.N., Bidigare, R.R., Kennicutt, M.C., Macko, S.A., 1995. Dependence of phytoplankton carbon isotopic composition on growth rate and $[CO_2]_{aq}$: theoretical considerations and experimental results. Geochim. Cosmochim. Acta 59, 1131–1135.

71. Lee C., Y.-L., & Chen, H.-Y. (2006). Seasonal dynamics of primary and new production in the northern South China Sea: The significance of river discharge and nutrient advection. *Deep-Sea Research Part I: Oceanographic Research Papers, 53*(6), 971–986. https://doi.org/10.1016/j.dsr.2006.02.005

72. Lee, D., Son, S., Joo, H., Kim, K., Kim, M.J., Jang, H.K., Yun, M.S., Kang, C.-K., Lee, S.H. (2020). Estimation of the particulate organic carbon to chlorophyll-a ratio using MODIS-aqua in the East/Japan sea, South Korea. *Remote Sens*. 12 (5), 840. http://dx.doi.org/10.3390/rs12050840.

73. Lee, J., Liu, J. T., Hung, C.-C., Lin, S., & Du, X. (2016). River plume-induced variability of suspended particle characteristics. *Marine Geology, 380*, 219–230. https://doi.org/10.1016/j.margeo.2016.04.014

74. Lee, J., Liu, J. T., Lee, I.-H., Fu, K.-H., Yang, R. J., Gong, W.-P., and Gan, J.-P. (2021). Encountering shoaling internal waves on the dispersal pathway of the Pearl River Plume in Summer. *Scientific Reports* 11 (1): 999. https://doi.org/10.1038/s41598-020-80215-2

75. Lee, J., Liu, J. T., Lin, Y.-S., Chen, C.-T. A., & Wang, B.-S. (2023). The contrast in suspended particle dynamics at surface and near bottom on the river-dominated northern South China Sea shelf in summer: Implication on physics and biogeochemistry coupling.

https://doi.org/10.5194/egusphere-2025-2502
Preprint. Discussion started: 21 July 2025

Frontiers in Marine Science, 10. https://www.frontiersin.org/journals/marine-science/articles/10.3389/fmars.2023.1156915

76. Li, Q. P., Zhou, W., Chen, Y., & Wu, Z. (2018). Phytoplankton response to a plume front in the northern South China Sea. *Biogeosciences, 15*(8), 2551–2563. https://doi.org/10.5194/bg-15-2551-2018

77. Li, Q. P., Ge, Z., Liu, Z., Zhou, W., Shuai, Y., & Wu, Z. (2021). Transparent exopolymer particles in a coastal frontal zone of the northern South China Sea and the associated biogeochemical implications. *Journal of Geophysical Research: Biogeosciences, 126*(2), e2020JG005893. https://doi.org/10.1029/2020JG005893

78. Liu, F., Chen, H., Cai, H., Luo, X., Ou, S., & Yang, Q. (2017). Impacts of ENSO on multi-scale variations in sediment discharge from the Pearl River to the South China Sea. *Geomorphology, 293*, 24–36. https://doi.org/10.1016/j.geomorph.2017.05.007

79. Liu, F., Hu, S., Guo, X., Luo, X., Cai, H., & Yang, Q. (2018a). Recent changes in the sediment regime of the Pearl River (South China): Causes and implications for the Pearl River Delta. *Hydrological Processes, 32*(12), 1771–1785. https://doi.org/10.1002/hyp.11513

80. Liu, H., Xue, B., Feng, Y., Zhang, R., Chen, M., & Sun, J. (2016). Size-fractionated chlorophyll-a biomass in the northern South China Sea in summer 2014. *Chinese Journal of Oceanology and Limnology, 34*(4), 672–682. https://doi.org/10.1007/s00343-016-5017-1

81. Liu, J. T., Hsu, R. T., Yang, R. J., Wang, Y. P., Wu, H., Du, X., Li, A., et al. (2018b). A comprehensive sediment dynamics study of a major mud belt system on the inner shelf along an energetic coast. *Scientific Reports, 8*(1), 4229. https://doi.org/10.1038/s41598-018-22696-w

82. Liu, J. T., Huang, B., Chang, Y., Du, X., Liu, X., Yang, R. J., Hsu, R. T., et al. (2019). Three-dimensional coupling between size-fractionated chlorophyll-a, POC and physical processes in the Taiwan Strait in summer. *Progress in Oceanography, 176*, 102129. https://doi.org/10.1016/j.pocean.2019.102129

83. Liu, J. T., Lee, J., Yang, R. J., Du, X., Li, A., Lin, Y.-S., Su, C.-C., & Tao, S. (2021). Coupling between physical processes and biogeochemistry of suspended particles over the inner shelf mud in the East China Sea. *Marine Geology, 442*, 106657. https://doi.org/10.1016/j.margeo.2021.106657

84. Liu, J., Yan, W., Chen, Z., & Lu, J. (2012). Sediment sources and their contribution along northern coast of the South China Sea: Evidence from clay minerals of surface

https://doi.org/10.5194/egusphere-2025-2502
Preprint. Discussion started: 21 July 2025

sediments. *Continental Shelf Research, 47*, 156–164. https://doi.org/10.1016/j.csr.2012.07.013

85. Liu, K.-K., Kao, S.-J., Hu, H.-C., Chou, W.-C., Hung, G.-W., & Tseng, C.-M. (2007). Carbon isotopic composition of suspended and sinking particulate organic matter in the northern South China Sea—From production to deposition. *Deep-Sea Research Part II: Topical Studies in Oceanography, 54*(14), 1504–1527. https://doi.org/10.1016/j.dsr2.2007.05.010

86. Liu, Q., Kandasamy, S., Lin, B., Wang, H., Chen, C.T.A., (2018c). Biogeochemical characteristics of suspended particulate matter in deep chlorophyll maximum layers in the southern East China Sea. *Biogeosciences* 15, 2091–2109.

87. Liu, Z., Colin, C., Li, X., Zhao, Y., Tuo, S., Chen, Z., Siringan, F. P., et al. (2010). Clay mineral distribution in surface sediments of the northeastern South China Sea and surrounding fluvial drainage basins: Source and transport. *Marine Geology, 277*(1), 48–60. https://doi.org/10.1016/j.margeo.2010.08.010

88. Lorenzoni, L., Thunell, R. C., Benitez-Nelson, C. R., Hollander, D., Martinez, N., Tappa, E., Varela, R., Astor, Y., & Muller-Karger, F. E. (2009). The importance of subsurface nepheloid layers in transport and delivery of sediments to the eastern Cariaco Basin, Venezuela. *Deep-Sea Research Part I: Oceanographic Research Papers, 56*(12), 2249–2262. https://doi.org/10.1016/j.dsr.2009.08.001

89. Lu, S., Wang, X., & Han, B. (2009). A field study on the conversion ratio of phytoplankton biomass carbon to chlorophyll-a in Jiaozhou Bay, China. *Chinese Journal of Oceanology and Limnology, 27*(4), 793–805. https://doi.org/10.1007/s00343-009-9221-0

90. Lu, Z., & Gan, J. (2015). Controls of seasonal variability of phytoplankton blooms in the Pearl River Estuary. *Deep-Sea Research Part II: Topical Studies in Oceanography, 117*, 86–96. https://doi.org/10.1016/j.dsr2.2013.12.011

91. Lu, Z., Gan, J., Dai, M., & Cheung, A. Y. Y. (2010). The influence of coastal upwelling and a river plume on the subsurface chlorophyll maximum over the shelf of the northeastern South China Sea. *Journal of Marine Systems, 82*(1), 35–46. https://doi.org/10.1016/j.jmarsys.2010.03.002

92. Luo, L., Li, S., & Wang, D. (2009). Hypoxia in the Pearl River Estuary, the South China Sea, in July 1999. *Aquatic Ecosystem Health & Management, 12*(4), 418–428. https://doi.org/10.1080/14634980903352407

https://doi.org/10.5194/egusphere-2025-2502
Preprint. Discussion started: 21 July 2025

93. Luo, L., & Wu, M. (2023). Spatiotemporal characteristics of summer hypoxia in Mirs Bay and adjacent coastal waters, South China. *Journal of Oceanology and Limnology, 41*(2), 482–494. https://doi.org/10.1007/s00343-022-2025-1

94. Lynn, R. J., & Reid, J. L. (1968). Characteristics and circulation of deep and abyssal waters. *Deep-Sea Research and Oceanographic Abstracts, 15*(5), 577–598. https://doi.org/10.1016/0011-7471(68)90064-8

95. Maes, C., & O'Kane, T. J. (2014). Seasonal variations of the upper ocean salinity stratification in the tropics. *Journal of Geophysical Research: Oceans, 119*(3), 1706–1722. https://doi.org/10.1002/2013JC009366

96. Manning, A. J., Langston, W. J., & Jonas, P. J. C. (2010). A review of sediment dynamics in the Severn Estuary: Influence of flocculation. *Marine Pollution Bulletin, 61*(1), 37–51. https://doi.org/10.1016/j.marpolbul.2009.12.012

97. Mari, X., Passow, U., Migon, C., Burd, A. B., & Legendre, L. (2017). Transparent exopolymer particles: Effects on carbon cycling in the ocean. *Progress in Oceanography, 151*, 13–37. https://doi.org/10.1016/j.pocean.2016.11.002

98. Meyers, P. A., & Eadie, B. J. (1993). Sources, degradation and recycling of organic matter associated with sinking particles in Lake Michigan. *Organic Geochemistry, 20*(1), 47–56. https://doi.org/10.1016/0146-6380(93)90080-U

99. Michels, J., Stippkugel, A., Lenz, M., Wirtz, K., & Engel, A. (2018). Rapid aggregation of biofilm-covered microplastics with marine biogenic particles. *Proceedings of the Royal Society B: Biological Sciences, 285*(1885), 20181203. https://doi.org/10.1098/rspb.2018.1203

100. Miller, T. W., Brodeur, R. D., & Rau, G. H. (2008). Carbon stable isotopes reveal relative contribution of shelf-slope production to the northern California Current pelagic community. *Limnology and Oceanography, 53*(4), 1493–1503. https://doi.org/10.4319/lo.2008.53.4.1493

101. Moser, S. C., Williams, S. J., & Boesch, D. F. (2012). Wicked challenges at land's end: Managing coastal vulnerability under climate change. *Annual Review of Environment and Resources, 37*(1), 51–78. https://doi.org/10.1146/annurev-environ-021611-135158

102. Mullin, J. B., & Riley, J. P. (1955). The colorimetric determination of silicate with special reference to sea and natural waters. *Analytica Chimica Acta, 12*, 162–176. https://doi.org/10.1016/S0003-2670(00)87825-3

https://doi.org/10.5194/egusphere-2025-2502
Preprint. Discussion started: 21 July 2025

103. Murphy, J., & Riley, J. P. (1962). A modified single solution method for the determination of phosphate in natural waters. *Analytica Chimica Acta, 27*, 31–36. https://doi.org/10.1016/S0003-2670(00)88444-5

104. Nakatsuka T., Handa N., Wada E., Wong C. (1992). The dynamic changes of stable isotopic ratios of carbon and nitrogen in suspended and sedimented particulate organic matter during a phytoplankton bloom. *Journal of Marine Research*, *50*(2), 267–296.

105. Neumann, G., & Pierson, W. J. (1966). *Principles of Physical Oceanography*. Prentice Hall: Englewood Cliffs, NJ.

106. Ning, X., Chai, F., Xue, H., Cai, Y., Liu, C., & Shi, J. (2004). Physical-biological oceanographic coupling influencing phytoplankton and primary production in the South China Sea. *Journal of Geophysical Research: Oceans, 109*(C10). https://doi.org/10.1029/2004JC002365

107. Ou, S., Yang, Q., Luo, X., Zhu, F., Luo, K., & Yang, H. (2019). The influence of runoff and wind on the dispersion patterns of suspended sediment in the Zhujiang (Pearl) River Estuary based on MODIS data. *Acta Oceanologica Sinica, 38*(3), 26–35. https://doi.org/10.1007/s13131-019-1396-4

108. Ou, S., Zhang, H., & Wang, D. (2009). Dynamics of the buoyant plume off the Pearl River Estuary in summer. *Environmental Fluid Mechanics, 9*(5), 471–492. https://doi.org/10.1007/s10652-009-9146-3

109. Ouyang, R., Liu, W., Fu, G., Liu, C., Hu, L., & Wang, H. (2014). Linkages between ENSO/PDO signals and precipitation, streamflow in China during the last 100 years. *Hydrology and Earth System Sciences, 18*(9), 3651–3661. https://doi.org/10.5194/hess-18-3651-2014

110. Pai, S.-C., Su, Y.-T., Lu, M.-C., Chou, Y., & Ho, T.-Y. (2021). Determination of nitrate in natural waters by vanadium reduction and the Griess assay: Reassessment and optimization. *ACS ES&T Water, 1*(6), 1524–1532. https://doi.org/10.1021/acsestwater.1c00065

111. Pai, S.-C., Yang, C.-C., & Riley, J. P. (1990a). Effects of acidity and molybdate concentration on the kinetics of the formation of the phosphoantimonylmolybdenum blue complex. *Analytica Chimica Acta, 229*, 115–120. https://doi.org/10.1016/S0003-2670(00)85116-8

112. Pai, S.-C., Yang, C.-C., & Riley, J. P. (1990b). Formation kinetics of the pink azo dye in the determination of nitrite in natural waters. *Analytica Chimica Acta, 232*, 345–349. https://doi.org/10.1016/S0003-2670(00)81252-0

https://doi.org/10.5194/egusphere-2025-2502
Preprint. Discussion started: 21 July 2025

113. Pan, J., Gu, Y., & Wang, D. (2014). Observations and numerical modeling of the Pearl River plume in summer season. *Journal of Geophysical Research: Oceans, 119*(4), 2480–2500. https://doi.org/10.1002/2013JC009042

114. Passow, U. (2002). Transparent exopolymer particles (TEP) in aquatic environments. Progr. Oceanogr. 55, 287–333. doi: 10.1016/S0079-6611(02)00138-6

115. Peng, J., Luo, X., Liu, F., & Zhang, Z. (2018). Analyzing the influences of ENSO and PDO on water discharge from the Yangtze River into the sea. *Hydrological Processes, 32*(8), 1090–1103. https://doi.org/10.1002/hyp.11484

116. Petersen, J. E., Sanford, L. P., & Kemp, W. M. (1998). Coastal plankton responses to turbulent mixing in experimental ecosystems. *Marine Ecology Progress Series, 171*, 23–41. https://www.int-res.com/abstracts/meps/v171/p23-41/

117. Phillips, D. L., Newsome, S. D., & Gregg, J. W. (2005). Combining sources in stable isotope mixing models: Alternative methods. *Oecologia, 144*(4), 520–527. https://doi.org/10.1007/s00442-004-1816-8

118. Qian, W., Gan, J., Liu, J., He, B., Lu, Z., Guo, X., Wang, D., Guo, L., Huang, T., & Dai, M. (2018). Current status of emerging hypoxia in a eutrophic estuary: The lower reach of the Pearl River Estuary, China. *Estuarine, Coastal and Shelf Science, 205*, 58–67. https://doi.org/10.1016/j.ecss.2018.03.004

119. Quay, P., & Wu, J. (2015). Impact of end-member mixing on depth distributions of $\Delta^{13}C$, cadmium and nutrients in the N. Atlantic Ocean. *Deep-Sea Research Part II: Topical Studies in Oceanography, 116*, 107–116. https://doi.org/10.1016/j.dsr2.2014.11.009

120. Ren, J., Li, W., & Gao, Y. (2020). Analyzing dynamic characteristics of river plume in the Modaomen Mouth, Pearl River Estuary. *Journal of Oceanography, 76*(4), 247–258. https://doi.org/10.1007/s10872-020-00542-w

121. Rimmelin, P., & Moutin, T. (2005). Re-examination of the MAGIC method to determine low orthophosphate concentration in seawater. *Analytica Chimica Acta, 548*(1), 174–182. https://doi.org/10.1016/j.aca.2005.05.071

122. Schnetger, B., & Lehners, C. (2014). Determination of nitrate plus nitrite in small volume marine water samples using vanadium(III) chloride as a reduction agent. *Marine Chemistry, 160*, 91–98. https://doi.org/10.1016/j.marchem.2014.01.010

123. SCOR Working Group. (2007). GEOTRACES – An international study of the global marine biogeochemical cycles of trace elements and their isotopes. Geochemistry, 67(2), 85–131. https://doi.org/10.1016/j.chemer.2007.02.001

https://doi.org/10.5194/egusphere-2025-2502
Preprint. Discussion started: 21 July 2025

124. Shi, W., & Wang, M. (2009). Satellite observations of flood-driven Mississippi River plume in the spring of 2008. *Geophysical Research Letters, 36*(7). https://doi.org/10.1029/2009GL037210

125. Shu, Y., Chen, J., Yao, J., Pan, J., Wang, W., Mao, H., & Wang, D. (2014). Effects of the Pearl River plume on the vertical structure of coastal currents in the northern South China Sea during summer 2008. *Ocean Dynamics, 64*(12), 1743–1752. https://doi.org/10.1007/s10236-014-0779-5

126. Strickland, J. D. H., & Parsons, T. R. (1972). *A practical handbook of seawater analysis* (2nd ed., Vol. 167). Fisheries Research Board of Canada, Ottawa, Canada. https://doi.org/10.25607/OBP-1791

127. Su, J. (2004). Overview of the South China Sea circulation and its influence on the coastal physical oceanography outside the Pearl River Estuary. *Continental Shelf Research, 24*(16), 1745–1760. https://doi.org/10.1016/j.csr.2004.06.005

128. Sun, X., Fan, D., Cheng, P., Hu, L., Sun, X., Guo, Z., & Yang, Z. (2021). Source, transport and fate of terrestrial organic carbon from Yangtze River during a large flood event: Insights from multiple-isotopes ($\Delta^{13}C$, $\Delta^{15}N$, $\Delta^{14}C$) and geochemical tracers. *Geochimica et Cosmochimica Acta, 308*, 217–236. https://doi.org/10.1016/j.gca.2021.06.004

129. Tao, S., Liu, J. T., Wang, A., Blattmann, T. M., Yang, R. J., Lee, J., Xu, J. J., et al. (2022). Deciphering organic matter distribution by source-specific biomarkers in the shallow Taiwan Strait from a source-to-sink perspective. *Frontiers in Marine Science, 9*. https://doi.org/10.3389/fmars.2022.969461

130. Taylor, A. H., Geider, R. J., & Gilbert, F. J. (1997). Seasonal and latitudinal dependencies of phytoplankton carbon-to-chlorophyll a ratios: Results of a modelling study. *Marine Ecology Progress Series, 152*, 51–66. https://www.int-res.com/abstracts/meps/v152/p51-66/

131. Tian, Y., Chen, Z., Hou, Z., Luo, Y., Xu, A., & Yan, W. (2019). Geoacoustic provinces of the northern South China Sea based on sound speed as predicted from sediment grain sizes. *Marine Geophysical Research, 40*(4), 571–579. https://doi.org/10.1007/s11001-019-09387-5

132. Tian, Z., Liu, Y., Zhang, X., Zhang, Y., & Zhang, M. (2022). Formation mechanisms and characteristics of the marine nepheloid layer: A review. *Water (Switzerland)*. MDPI. https://doi.org/10.3390/w14050678

https://doi.org/10.5194/egusphere-2025-2502
Preprint. Discussion started: 21 July 2025

133. Tong, Z., Ma, L., Cai, S., Wang, L., Xiao, W., Huang, B., & Laws, E. A. (2023). Responses of phytoplankton communities to the effect of both river plume and coastal upwelling. *Journal of Geophysical Research: Biogeosciences, 128*(11), e2023JG007486. https://doi.org/10.1029/2023JG007486

134. Tong, Z., Wang, C., Lin, L., Ma, L., & Huang, B. (2024). Nutrient depletion and phytoplankton shifts driven by the Pearl River plume in the Taiwan Strait. *Frontiers in Marine Science, 11*. https://doi.org/10.3389/fmars.2024.1485670

135. Tuerena, R. E., Ganeshram, R. S., Humphreys, M. P., Browning, T. J., Bouman, H., & Piotrowski, A. P. (2019). Isotopic fractionation of carbon during uptake by phytoplankton across the South Atlantic Subtropical Convergence. *Biogeosciences, 16*(18), 3621–3635. https://doi.org/10.5194/bg-16-3621-2019

136. Turner, A., & Millward, G. E. (2002). Suspended particles: Their role in estuarine biogeochemical cycles. *Estuarine, Coastal and Shelf Science, 55*(6), 857–883. https://doi.org/10.1006/ecss.2002.1033

137. Voynova, Y. G., & Sharp, J. H. (2012). Anomalous biogeochemical response to a flooding event in the Delaware Estuary: A possible typology shift due to climate change. *Estuaries and Coasts, 35*(4), 943–958. https://doi.org/10.1007/s12237-012-9490-2

138. Wang, Y., Chen, X., Switzer, A. D., Li, L., Xu, Y., Wang, Y., & Zhang, P. (2023). Relict and modern sediments on the continental shelf of the northern South China Sea: A reconsideration. *Journal of Geophysical Research: Earth Surface, 128*(8), e2023JF007125. https://doi.org/10.1029/2023JF007125

139. Wang, Z., Hu, S., Li, Q., Liu, H., & Wu, G. (2022). Variability of marine particle size distributions and the correlations with inherent optical properties in the coastal waters of the northern South China Sea. *Remote Sensing, 14*(12). https://doi.org/10.3390/rs14122881

140. Weaver, B. L. (1991). The origin of ocean island basalt end-member compositions: Trace element and isotopic constraints. *Earth and Planetary Science Letters, 104*(2), 381–397. https://doi.org/10.1016/0012-821X(91)90217-6

141. Wei, B., Mollenhauer, G., Hefter, J., Grotheer, H., & Jia, G. (2020). Dispersal and aging of terrigenous organic matter in the Pearl River Estuary and the northern South China Sea shelf. *Geochimica et Cosmochimica Acta, 282*, 324–339. https://doi.org/10.1016/j.gca.2020.04.032

https://doi.org/10.5194/egusphere-2025-2502
Preprint. Discussion started: 21 July 2025

142. Wei, X., Cai, S., Zhan, W. (2021). Impact of anthropogenic activities on morphological and deposition flux changes in the Pearl River estuary, *China. Sci. Rep.* 11 (1) https://doi.org/10.1038/s41598-021-96183-0.

143. Williams, C., Sharples, J., Green, M., Mahaffey, C., & Rippeth, T. (2013). The maintenance of the subsurface chlorophyll maximum in the stratified western Irish Sea. *Limnology and Oceanography: Fluids and Environments, 3*(1), 61–73. https://doi.org/10.1215/21573689-2285100

144. Wong, G. T. F., Pan, X., Li, K.-Y., Shiah, F.-K., Ho, T.-Y., & Guo, X. (2015). Hydrography and nutrient dynamics in the northern South China Sea shelf-sea (NoSoCS). *Deep-Sea Research Part II: Topical Studies in Oceanography, 117*, 23–40. https://doi.org/10.1016/j.dsr2.2015.02.023

145. Xia, X. M., Li, Y., Yang, H., Wu, C. Y., Sing, T. H., & Pong, H. K. (2004). Observations on the size and settling velocity distributions of suspended sediment in the Pearl River Estuary, China. *Continental Shelf Research, 24*(16), 1809–1826. https://doi.org/10.1016/j.csr.2004.06.009

146. Xiao, M., Zhang, Q., Singh, V. P., & Liu, L. (2016). Transitional properties of droughts and related impacts of climate indices in the Pearl River Basin, China. *Journal of Hydrology, 534*, 397–406. https://doi.org/10.1016/j.jhydrol.2016.01.012

147. Xie, Y., Lin, L., Xiao, W., Yu, X., Lan, W., & Huang, B. (2020). Striking seasonal pattern of primary production in the river-dominated ocean margin of the northern South China Sea (NSCS-RiOMar) revealed by new field and remotely sensed data. *Progress in Oceanography, 189*, 102470. https://doi.org/10.1016/j.pocean.2020.102470

148. Xu, C., Xu, Y., Hu, J., Li, S., & Wang, B. (2019). A numerical analysis of the summertime Pearl River plume from 1999 to 2010: Dispersal patterns and intraseasonal variability. *Journal of Marine Systems, 192*, 15–27. https://doi.org/10.1016/j.jmarsys.2018.12.010

149. Xu, J., Yin, K., He, L., Yuan, X., Ho, A. Y. T., & Harrison, P. J. (2008). Phosphorus limitation in the northern South China Sea during late summer: Influence of the Pearl River. *Deep-Sea Research Part I: Oceanographic Research Papers, 55*(10), 1330–1342. https://doi.org/10.1016/j.dsr.2008.05.007

150. Xu, W., Wang, G., Cheng, X., Jiang, L., Zhou, W., & Cao, W. (2022). Characteristics of subsurface chlorophyll maxima during the boreal summer in the South China Sea with respect to environmental properties. *Science of The Total Environment, 820*, 153243. https://doi.org/10.1016/j.scitotenv.2022.153243

https://doi.org/10.5194/egusphere-2025-2502
Preprint. Discussion started: 21 July 2025

151. Yang, R. J., Liu, J. T., Su, C.-C., Chang, Y., Xu, J. J., & Lui, H.-K. (2021). Land-ocean interaction affected by the monsoon regime change in western Taiwan Strait. *Frontiers in Marine Science, 8*. https://doi.org/10.3389/fmars.2021.735242

152. Yin, K., Qian, P.-Y., Wu, M. C. S., Chen, J. C., Huang, L., Song, X., & Jian, W. (2001). Shift from P to N limitation of phytoplankton growth across the Pearl River Estuarine Plume during summer. *Marine Ecology Progress Series, 221*, 17–28. http://www.jstor.org/stable/24865282

153. Yin, K., Zhang, J., Qian, P.-Y., Jian, W., Huang, L., Chen, J., & Wu, M. C. S. (2004). Effect of wind events on phytoplankton blooms in the Pearl River Estuary during summer. *Continental Shelf Research, 24*(16), 1909–1923. https://doi.org/10.1016/j.csr.2004.06.015

154. Yu, X., Xu, J., Long, A., Li, R., Shi, Z., & Li, Q. P. (2020). Carbon-to-chlorophyll ratio and carbon content of phytoplankton community at the surface in coastal waters adjacent to the Zhujiang River Estuary during summer. *Acta Oceanologica Sinica, 39*(2), 123–131. https://doi.org/10.1007/s13131-020-1556-6

155. Zeng, L., Wang, D., Chen, J., Wang, W., & Chen, R. (2016). SCSPOD14, a South China Sea physical oceanographic dataset derived from in situ measurements during 1919–2014. *Scientific Data, 3*(1), 160029. https://doi.org/10.1038/sdata.2016.29

156. Zhang, J., Yu, Z. G., Wang, J. T., Ren, J. L., Chen, H. T., Xiong, H., Dong, L. X., & Xu, W. Y. (1999). The subtropical Zhujiang (Pearl River) Estuary: Nutrient, trace species and their relationship to photosynthesis. *Estuarine, Coastal and Shelf Science, 49*(3), 385–400. https://doi.org/10.1006/ecss.1999.0500

157. Zhang, Q., Gu, X., Singh, V. P., Xiao, M., & Xu, C.-Y. (2015). Flood frequency under the influence of trends in the Pearl River Basin, China: Changing patterns, causes and implications. *Hydrological Processes, 29*(6), 1406–1417. https://doi.org/10.1002/hyp.10278

158. Zhang, W., Mu, S., Zhang, Y., & Chen, K.-M. (2012). Seasonal and interannual variations of flow discharge from Pearl River into sea. *Water Science and Engineering, 5*(4), 399–409. https://doi.org/10.3882/j.issn.1674-2370.2012.04.004

159. Zhong, Q., Xue, B., Noman, M. A., Wei, Y., Liu, H., Liu, H., Zheng, L., Jing, H., & Sun, J. (2021). Effect of river plume on phytoplankton community structure in Zhujiang River Estuary. *Journal of Oceanology and Limnology, 39*(2), 550–565. https://doi.org/10.1007/s00343-020-9213-7

https://doi.org/10.5194/egusphere-2025-2502
Preprint. Discussion started: 21 July 2025

160. Zhou, L., Huang, L., Tan, Y., Lian, X., & Li, K. (2015). Size-based analysis of a zooplankton community under the influence of the Pearl River plume and coastal upwelling in the northeastern South China Sea. *Marine Biology Research, 11*(2), 168–179. https://doi.org/10.1080/17451000.2014.904882

161. Zhou, W., Wang, D., & Luo, L. (2012). Investigation of saltwater intrusion and salinity stratification in winter of 2007/2008 in the Zhujiang River Estuary in China. *Acta Oceanologica Sinica, 31*(3), 31–46. https://doi.org/10.1007/s13131-012-0204-1

162. Zhou, Z., Shi, H., Fu, Q., Ding, Y., Li, T., Wang, Y., & Liu, S. (2021). Characteristics of propagation from meteorological drought to hydrological drought in the Pearl River Basin. *Journal of Geophysical Research: Atmospheres, 126*(4), e2020JD033959. https://doi.org/10.1029/2020JD033959

163. Zu, T., & Gan, J. (2015). A numerical study of coupled estuary–shelf circulation around the Pearl River Estuary during summer: Responses to variable winds, tides and river discharge. *Deep-Sea Research Part II: Topical Studies in Oceanography, 117*, 53–64. https://doi.org/10.1016/j.dsr2.2013.12.010

164. Zu, T., Wang, D., Gan, J., & Guan, W. (2014). On the role of wind and tide in generating variability of Pearl River plume during summer in a coupled wide estuary and shelf system. *Journal of Marine Systems, 136*, 65–79. https://doi.org/10.1016/j.jmarsys.2014.03.005